Author Manuscript

Author Manuscript

Author Manuscript

Author Manuscript

HHS Public Access

Author manuscript

Cell Rep. Author manuscript; available in PMC 2019 January 23.

Published in final edited form as:

Cell Rep. 2019 January 08; 26(2): 483–495.e5. doi:10.1016/j.celrep.2018.12.042.

An Allosteric Interaction Network Promotes Conformation State-Dependent Eviction of the Nas6 Assembly Chaperone from Nascent 26S Proteasomes

Antonia A. Nemec[1], **Anna K. Peterson**[1], **Jennifer L. Warnock**[1], **Randi G. Reed**[1], and **Robert J. Tomko Jr.**[1,2,*]

[1]Department of Biomedical Sciences, Florida State University College of Medicine, 1115 W. Call St., Tallahassee, FL 32306, USA

[2]Lead Contact

SUMMARY

The 26S proteasome is the central ATP-dependent protease in eukaryotes and is essential for organismal health. Proteasome assembly is mediated by several dedicated, evolutionarily conserved chaperone proteins. These chaperones associate transiently with assembly intermediates but are absent from mature proteasomes. Chaperone eviction upon completion of proteasome assembly is necessary for normal proteasome function, but how they are released remains unresolved. Here, we demonstrate that the Nas6 assembly chaperone, homolog of the human oncogene gankyrin, is evicted from nascent proteasomes during completion of assembly via a conformation-specific allosteric interaction of the Rpn5 subunit with the proteasomal ATPase ring. Subsequent ATP binding by the ATPase subunit Rpt3 promotes conformational remodeling of the ATPase ring that evicts Nas6 from the nascent proteasome. Our study demonstrates how assembly-coupled allosteric signals promote chaperone eviction and provides a framework for understanding the eviction of other chaperones from this bio-medically important molecular machine.

Graphical Abstract

This is an open access article under the CC BY-NC-ND license (http://creativecommons.org/licenses/by-nc-nd/4.0/).

*Correspondence: robert.tomko@med.fsu.edu.

AUTHOR CONTRIBUTIONS

A.A.N. and R.J.T. conceived the study. R.J.T. and A.K.P. generated yeast strains. A.A.N. and R.J.T. generated plasmids. A.A.N., A.K.P., and R.J.T. purified proteins. A.A.N. performed most biochemical and genetic experiments. J.L.W. performed genetic experiments. R.G.R. performed crosslinking experiments. R.J.T. performed all modeling. A.A.N. wrote the first draft of the manuscript, and all authors provided feedback. R.J.T. supervised the study and edited the manuscript.

SUPPLEMENTAL INFORMATION

Supplemental Information includes six figures and six tables and can be found with this article online at https://doi.org/10.1016Zj.celrep.2018.12.042.

DECLARATION OF INTERESTS

The authors declare no competing interests.

Author Manuscript Author Manuscript Author Manuscript Author Manuscript

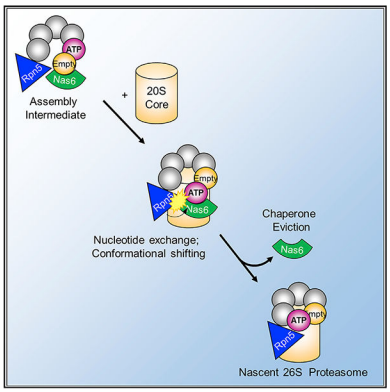

In Brief

Nemec et al. report how the evolutionarily conserved Nas6 assembly chaperone is evicted from nascent 26S proteasomes. Nucleotide binding events within the nascent proteasome trigger formation of conformation-specific intersubunit contacts that expel Nas6. This mechanism may serve a quality control function by blocking formation of 26S proteasomes from defective components.

INTRODUCTION

The ubiquitin-proteasome system (UPS) clears damaged or unneeded proteins from cells and is deregulated in numerous human diseases (Schmidt and Finley, 2014; Tomko and Hochstrasser, 2013). UPS substrates are typically first modified with a chain of the small protein ubiquitin, which serves as a signal for delivery to the 26S proteasome, a 2.5 MDa ATP-dependent protease complex. The 26S proteasome consists of a barrel-shaped 20S core particle (CP) that is capped on one or both ends by the 19S regulatory particle (RP). The RP can be further divided into lid and base subcomplexes (Figure 1A). The lid consists of nine subunits: Rpn3, Rpn5–Rpn9, Rpn11, Rpn12, and Sem1/Rpn15. The base consists of a heterohexameric ring of six AAA+ ATPases, Rpt1–Rpt6, and the non-ATPase subunits Rpn1, Rpn2, and Rpn13. The lid removes the polyubiquitin targeting signal from the substrate via the deubiquitinase subunit Rpn11. The base uses mechanical force derived from ATP to unfold the substrate and translocate it into the CP, where it is cleaved into short peptides.

In humans and yeast, the 26S proteasome adopts several conformational states (Chen et al., 2016; Eisele et al., 2018; Guo et al., 2018; Huang et al., 2016; Luan et al., 2016; Matyskiela et al., 2013; Śledź et al., 2013; Unverdorben et al., 2014; Wehmer et al., 2017; Zhu et al., 2018) that can be separated into a substrate free state (herein called s1) and several closely related substrate processing states (herein called s3-like states) (reviewed in Bard et al., 2018). The s1 state is a resting, inactive state in which the substrate passageways are occluded and the active site of the deubiquitinase subunit Rpn11 is shielded from the substrate. The s3-like states are highly similar to one another and are distinguished by the alignment of the substrate passageways and a large rotation of the lid subcomplex that positions Rpn11 over the ATPase pore to allow for cotranslocational deubiquitination of

Author Manuscript Author Manuscript Author Manuscript Author Manuscript

substrates (dela Peña et al., 2018; Matyskiela et al., 2013). Although conformational analyses have greatly enhanced our understanding of proteasomal substrate processing, less is known about how conformational rearrangements contribute to proteasome assembly (Dambacher et al., 2016; Kock et al., 2015; Tomko et al., 2015; Wani et al., 2015).

Proteasome assembly is a conserved process that depends upon both intrinsic subunit features and extrinsic assembly chaperones (Howell et al., 2017). The lid, base, and CP can assemble independent of one another, although the base likely can also assemble using the CP as a scaffold (Kusmierczyk et al., 2008; Park et al., 2009). Under physiological conditions, base assembly is controlled by four dedicated, evolutionarily conserved assembly chaperones: Nas6, Rpn14, Hsm3, and Nas2 (Funakoshi et al., 2009; Kaneko et al., 2009; Le Tallec et al., 2009; Park et al., 2009; Roelofs et al., 2009; Saeki et al., 2009). An inducible chaperone, Adc17, enhances base assembly under stress conditions in yeast (Hanssum et al., 2014). Each of the four dedicated chaperones binds the C-terminal domain of a specific Rpt subunit in a pairwise manner to form the intermediate complexes Nas6-Rpt3-Rpt6-Rpn14, Hsm3-Rpt1-Rpt2-Rpn1, and Rpt4-Rpt5-Nas2. These intermediates then assemble in an ordered fashion (Kaneko et al., 2009; Tomko et al., 2010), along with Rpn2 and Rpn13 (Tomko and Hochstrasser, 2011), to produce the base.

Much progress has been made toward understanding how base assembly chaperones promote proteasome biogenesis (reviewed in Howell et al., 2017). Generally, the four constitutive base chaperones prevent premature docking of proteasomal ATPases onto the surface of the CP by providing a steric blockade of the interaction surface. Furthermore, individual chaperones serve distinct roles during assembly. Hsm3 stabilizes the Rpt1-Rpt2-Rpn1 intermediate during assembly (Barrault et al., 2012), and Nas2 prevents premature interaction of the Rpt4-Rpt5-Nas2 and Hsm3-Rpt1-Rpt2-Rpn1 modules (Satoh et al., 2014; Tomko et al., 2010). Nas6 was reported to restrict association of the lid and CP with the base in a nucleotide-dependent manner, suggesting that nucleotide binding or hydrolysis events are tied to the association of the three major proteasomal subcomplexes (Li et al., 2017). However, the detailed molecular mechanisms regulating the association of the lid, base, and CP during proteasome biogenesis remain unclear.

A fundamental question that remains unanswered is how the base chaperones are released from the nascent 26S proteasome upon completion of assembly. Such eviction is necessary for proper proteasome function. It is thought that formation of a transient RP-chaperone-CP complex must occur to complete 26S proteasome assembly and promote eviction of the chaperones (Li et al., 2017; Lu et al., 2017). Although early molecular modeling studies conducted with homolog models of the base ATPase ring suggested that Nas6 and the CP were in full steric conflict (Park et al., 2013; Roelofs et al., 2009), a recent structure of the human RP bound by the Nas6 ortholog gankyrin demonstrated that a ternary complex of the fully assembled RP, CP, and gankyrin could form without obvious steric conflict (Lu et al., 2017). This is due to a pronounced opening of the nucleotide binding pocket of Rpt3 in the gankyrin-bound RP that is not present in cryo-electron microscopy (cryo-EM) structures of the chaperone-free 26S proteasome. We thus considered the possibility that conformational changes within the RP, likely triggered by nucleotide binding and/or hydrolysis, mediate eviction of Nas6 upon association of the RP and CP.

Author Manuscript Author Manuscript Author Manuscript Author Manuscript

In this study, we demonstrate that formation of a conformation-specific contact point between Rpn5 and the base promotes ATP-dependent conformational changes in Rpt3 that drive eviction of Nas6 from nascent proteasomes. These findings unite previous biochemical and structural studies and demonstrate allosteric communication between the lid and the CP during 26S proteasome assembly using the base as a conduit. Our results raise the intriguing possibility that chaperone eviction functions as a checkpoint to protect against the formation of 26S proteasomes from conformationally or functionally defective RPs.

RESULTS

Modeling Reveals Steric Clash between Rpn5 and Nas6 in Mature 26S Proteasomes

Six major conformational states, named s1–s6, of the mature yeast 26S proteasome have been reported (de la Peña et al., 2018; Eisele et al., 2018; Luan et al., 2016; Matyskiela et al., 2013; Śledź et al., 2013; Unverdorben et al., 2014; Wehmer et al., 2017). The mechanism(s) of interconversion among these states are uncertain, but the nucleotide state of the base ATPase ring heavily influences the conformational distribution (Eisele et al., 2018; Śledź et al., 2013; Zhu et al., 2018). To understand how conformational changes may affect interaction between Nas6 and the assembling proteasome, we superimposed the Nas6-Rpt3 co-complex (Nakamura et al., 2007) onto each state of the mature 26S proteasome. Steric clash was evident between Nas6 and lid subunit Rpn5 in all states examined (Figures 1B and 1C; Figures S1A–S1D), with the Rpn5 clash being particularly prominent in the s1 state (Figure 1B) and the s3 state (Figure 1C). We quantified the magnitude of clash between Nas6 and either the CP α ring or Rpn5 in each state (Table S3) and found that the s1 state uniquely showed strong steric clash of Nas6 with both Rpn5 and the CP (Figure S1; Table S3). In contrast, gankyrin showed no steric clash with Rpn5 in structures of the RP-gankyrin complex (Figure 1D; Figures S1E and S1F) (Lu et al., 2017). This is due to a widened gap between Rpt4 and Rpt3 that allows for simultaneous interaction of Rpn5 with Rpt4 and Nas6 with Rpt3. In addition, the surface of Rpn5 that contacts Rpt4 in the RP-gankyrin complex is distinct from the contacts between Rpn5 and the base in the s1–s6 states. Thus, we hypothesized that formation of state-specific contacts between Rpn5 and the ATPase ring upon RP-CP docking may regulate proteasome assembly.

Conformation-Specific Interaction between Rpn5 and the Base Controls RP-CP Association

Given the prominent clash between Nas6 and Rpn5 in the s1 and s3 states, we first aimed to introduce mutations that disrupted the contact points observed between Rpn5 and the base in either the s1 state or the s3 state. We identified residues E127, N128, and K129 in Rpn5 as making contact with the base subunits Rpt4 and Rpt3 in the s1 state, but not the s3 state (Figure 2A, yellow spheres). Similarly, we identified Rpn5 residues V198, R201, and K205 as making contact with the base via Rpt4 in the s3 state, but not the s1 state (Figure 2A, red spheres). We generated conformation-selective *RPN5* E127F/N128W/K129A mutant (*rpn5-s1mut*) and V198W/R201F/K205R mutant (*rpn5-s3mut*, which also disrupts Rpn5 contacts in the s3-like s4 and s6 states) (Table S3) alleles, with the expectation that they would disrupt Rpn5 contact with the base in these states without globally disrupting RP structure or conformational distribution.

Author Manuscript Author Manuscript Author Manuscript Author Manuscript

The *rpn5-s1mut* and *rpn5-s3mut* protein products were expressed at levels similar to those of wild-type (WT) Rpn5 (Figure S2A), cells harboring the mutants displayed no obvious growth defects at 30°C (Figure S2B), and the RP of *rpn5-s1mut* and *rpn5-s3mut* 26S proteasomes displayed no gross conformational or structural abnormalities based on conformation-specific crosslinking (Figure S2C) (Eisele et al., 2018). However, native PAGE of whole-cell extracts and immunoblotting against components of the lid, base, and CP revealed a loss of doubly capped proteasomes (RP_2CP) in *rpn5-s1mut* extracts (Figure 2B) that was accompanied by the accumulation of free CP and the appearance of a new species, which we term RP*. RP* was reactive with both lid and base subunit antibodies and migrated similarly to free RP. This unexpectedly suggested that the *rpn5-s1mut* mutations located at the Rpn5-base interface instead disrupted RP-CP interaction.

In support of a defect in RP-CP interaction, *rpn5-s1mut* displayed synthetic accumulation of RP* when combined with truncations of the C termini of Rpt3 and Rpt5 (Figure 2C; Figure S2D), which contain conserved motifs that dock into the surface of the CP to mediate stable RP-CP interaction (Smith et al., 2007). A similar phenotype was observed upon combination with a truncation of the Rpt6 C terminus, which has previously been linked to proteasome assembly (Park et al., 2009; Sokolova et al., 2015). Despite obvious steric clash with Nas6 in our modeling (Figure 1C), no impact was observed on proteasome assembly state or RP_2CP levels in *rpn5-s3mut* extracts (Figure 2B). However, this mutant accumulated polyubiquitin conjugates (Figure S2E) and displayed synthetic growth defects when combined with mutations in other proteasome subunits (Figure S2F), indicating these structure-guided mutations were effective. Because *rpn5-s3mut* also disrupts the Rpn5 contacts in the s4 and s6 states, we conclude that the s3, s4, and s6 Rpn5-base contacts are dispensable for RP-CP stability, whereas the s1 Rpn5-base contact is important.

We performed genetic analysis to support the importance of the Rpn5 s1 contact. Combination of the *rpn5-s1* mutation with a deletion of RP subunit gene *RPN10* yielded a synthetic growth defect at elevated temperature (Figure 2D). Rpn10 reinforces the RP structure and serves as a ubiquitin receptor. The observed growth defect was related to its structural role, because an inactivating mutation in the Rpn10 ubiquitin-interacting motif (*rpn10-uim*) displayed no synthetic defect with *rpn5-s1mut*. Many proteasome hypomorphs display synthetic defects upon deletion of the proteasome subunit transcription factor *RPN4*. Combination of *rpn5-s1mut* with *rpn4Δ* was lethal at elevated temperatures (Figure 2E), and examination of extracts from *rpn5-s1mut rpn4Δ* double-mutant cells grown at permissive temperature revealed an exacerbation of the *rpn5-s1mut* defect (Figure 2F; Figure S2G). Because Rpn4-dependent enhancement of proteasome assembly often compensates for assembly defects via mass action (Funakoshi et al., 2009; Tomko and Hochstrasser, 2014), this supports a role for the s1 Rpn5-base contact in RP-CP assembly.

The *rpn5-s1mut* RP-CP Defect Is Not Solely due to Disruption of Rpn5-CP Contact

Rpn5 makes direct contact with the CP in all six reported yeast 26S proteasome conformational states. This contact is strongest in the s1 state and appears to consist of a network of salt bridges formed by conserved amino acids Rpn5 E43/K44/K85 and α1 E250/D252 (Unverdorben et al., 2014) (Figures 3A–3C). We considered the possibility that *rpn5-*

Author Manuscript Author Manuscript Author Manuscript Author Manuscript

s1mut was indirectly causing repulsion of Rpn5 from the CP to yield the observed defect. To test this possibility, we generated an allele of *RPN5* in which E43, K44, and K85 were mutated to phe, phe, and ala, respectively (*rpn5-FFA*). We also generated an *α1(E250A)* allele in an attempt to disrupt the CP-side contacts. We observed formation of a small amount of RP* in immunoblots of native PAGE-separated extracts of *rpn5-FFA* or *α1(E250A)* yeast that was substantially less than that observed in *rpn5-s1mut* extracts. Combination of E250A with either *rpn5-FFA* or *rpn5-s1mut* did not further enhance RP* formation (Figure 3D; Figure S3A). Similar results were observed with various α1 D252 mutants (data not shown), suggesting that these mutations had minimal impact on RP-CP stability, possibly due to limited impact on Rpn5-CP contact. In contrast, truncation of the first 173 amino acids of Rpn5 (*Δ173-rpn5*), which removes the s1 Rpn5-base contact point, as well as the s1 Rpn5-CP contact, phenocopied the *rpn5-s1mut* defect (Figure 3E; Figure S3B). The *rpn5-FFA* mutant displayed a greater growth defect at elevated temperatures than the *rpn5-s1mut*, although less so than *Δ173-rpn5* (Figure 3F). Because mutations to Rpn5 partially suppressed peptidase activation in our hands (Figure S3C), this may reflect an important role for this contact in promoting gating or allosteric activation of the CP. Although these data suggest that disrupting the Rpn5-CP contact may cause a modest RP-CP defect, they cumulatively suggest that disruption of Rpn5 contact with the base, rather than with the CP, is primarily responsible for the observed *rpn5-s1mut* assembly defect.

The Base Assembly Chaperone Nas6 Is Required for the *rpn5-s1mut* Assembly Defect

We next investigated the composition of RP* by mass spectrometry. To purify RP*, we generated a strain expressing rpn5-s1mut-3×FLAG. The tag had no effect on the accumulation or abundance of RP* (data not shown). We then purified Rpn5-containing complexes via anti-FLAG affinity, eluted them under gentle conditions with excess 3×FLAG peptide, and resolved them by native PAGE. Next, we excised the band corresponding to RP* (and the same region from an untagged *rpn5-s1mut* purification as control) and subjected them to liquid chromatography-tandem mass spectrometry (LC-MS/MS) peptide sequencing. As expected, RP* contained all known subunits of the lid and base (Figure 4A and inset; Tables S4 and S5). However, this species also contained a sole RP assembly chaperone, Nas6. In agreement, Nas6, but not the Rpn14, Nas2, or Hsm3 RP assembly chaperones, immunopurified RP* readily from *rpn5-s1mut* extracts, as gauged by native PAGE immunoblotting (Figure 4B). In contrast, all expected chaperones were present on RP purified from RPN5–6×Gly-3×FLAG cells (Figure S4B; Table S6). The accumulation of Nas6 on RP in *rpn5-s1mut* cells was not due to enhanced expression of Nas6, because the steady-state protein levels were indistinguishable from those of WT cells (Figure S4A).

A simple explanation for the observed assembly defect and the enrichment of Nas6 on RP in *rpn5-s1mut* yeast is that Nas6 cannot be effectively evicted from *rpn5-s1mut* proteasomes during assembly and it instead destabilizes the RP-CP interface. As a first test of this hypothesis, we asked whether Nas6 was required for the *rpn5-s1mut* defect. We purified Nas6-free base (*nas6Δ* yBase) (Figure S4C) containing the Rpn14 and Hsm3 chaperones (Nas2 dissociates before completion of RP assembly) (Kaneko et al., 2009; Tomko et al., 2010) from *nas6Δ* yeast. We then performed *in vitro* 26S proteasome assembly assays using purified CP, recombinant Rpn10, *nas6Δ* yBase, and recombinant lid harboring either WT

Author Manuscript Author Manuscript Author Manuscript Author Manuscript

Rpn5 or Rpn5 containing *rpn5-s1mut* (rpn5-s1mut lid) (Figure S4D). When *nas6Δ* yBase was preincubated with recombinant Nas6 and added to Rpn10, CP, and WT lid, proteasomes formed as efficiently as when Nas6 was omitted (Figure 4C). Proteasomes were also efficiently formed from rpn5-s1mut lid when Nas6 was omitted. However, when Nas6 was added before assembly of proteasomes with rpn5-s1mut lid, a substantial reduction in doubly and singly capped proteasomes was observed and was accompanied by an accumulation of free RP. Nas6 was bound to the accumulated RP (Figure S4E), as observed *in vivo*. This effect was specific for Nas6, because recombinant Rpn14 had no impact (Figure S4F). Thus, the RP-CP assembly defect observed in *rpn5-s1mut* yeast depends both on the presence of Nas6 and on perturbation of the Rpn5 s1 contact.

If the Rpn5 s1 contact with the base evicts Nas6 from nascent 26S proteasomes, then *NAS6* deletion would be expected to rescue the *rpn5-s1mut* defect and Nas6 overexpression would exacerbate it. As predicted, *NAS6* deletion fully suppressed the *rpn5-s1mut* defect *in vivo* (Figure 4D), and overexpression of Nas6 caused further reduction in doubly and singly capped proteasomes and increased accumulation of RP and CP (Figure 4E; Figure S4G) in immunoblots of native PAGE-separated extracts of *rpn5-s1mut* yeast. Nas6 overexpression in WT yeast caused some accumulation of RP but no loss of 26S proteasomes, suggesting that Nas6 overproduction may drive further RP assembly by mass action but does not cause appreciable RP-CP dissociation when Rpn5 is WT, in agreement with our *in vitro* assays (Figure 4C). Consistent with the Nas6-dependent *rpn5-s1mut* defect, overexpression of Nas6, but not other chaperones, caused a severe growth defect in *rpn5-s1mut* yeast at elevated temperatures on media with the protein-destabilizing amino acid analog *L*-canavanine (Figure 4F). Altogether, these data indicate the Rpn5 s1 contact functionally opposes Nas6 during 26S proteasome assembly.

Rpn5 s1 Mutations Compromise Eviction of Nas6 from Nascent 26S Proteasomes

Formation of the Rpn5 s1 contact may stabilize 26S proteasomes by promoting eviction of Nas6 from nascent 26S proteasomes upon completion of assembly, by preventing Nas6 from rebinding and dissociating mature proteasomes into RP and CP, or both. If the Rpn5 s1 contact prevents rebinding of Nas6 to mature proteasomes, then addition of Nas6 to preassembled *rpn5-s1mut* proteasomes would promote their dissociation into RP and CP. We thus asked whether adding Nas6 to preassembled proteasomes compromised their stability. We either incubated *nas6Δ* yBase with recombinant Nas6 before *in vitro* assembly of 26S proteasomes, as in Figure 4, or assembled 26S proteasomes and then incubated them with Nas6. We ensured that the total time during which all components necessary for assembly were present was the same in both schemes. As before, preaddition of Nas6 to the base prevented efficient assembly of doubly and singly capped proteasomes from rpn5-s1mut lid (Figure 5A, lanes 5 and 6), whereas no impairment of 26S proteasome assembly was observed with WT lid (Figure 5A, lanes 2 and 3). When Nas6 was added to proteasomes containing rpn5-s1mut lid after assembly had been initiated, RP_2CP were present at the same abundance as for WT lid or for rpn5-s1mut lid in the absence of Nas6 (Figure 5A, lanes 5 and 7). This suggests that Nas6 must be present before completion of assembly to impair RP-CP interaction. Singly capped *rpn5-s1mut* proteasomes were slightly less abundant, and some accumulation of RP was observed even when Nas6 was added after

Author Manuscript Author Manuscript Author Manuscript Author Manuscript

assembly had initiated. This could be due to either incomplete assembly under our conditions or some modest disassembly of 26S proteasomes by Nas6 (as described later).

We used an enzymatic approach to confirm the results of our native PAGE-based analysis. We measured turnover of excess model proteasome substrate Ub_4-GFP-Tail by *in vitro*-assembled proteasomes under steady-state conditions. Proteasomes assembled from recombinant lid and *nas6Δ* yBase degraded this substrate with kinetics similar to purified yeast 26S proteasomes, and Ub_4-GFP-Tail was not turned over by reconstituted proteasomes lacking lid (Figure S5), indicating substrate turnover was mediated only by fully assembled 26S proteasomes. Because 26S proteasomes remain intact during substrate degradation (Kriegenburg et al., 2008), the linear degradation rate observed under steady-state conditions indicated that proteasome assembly was complete and not continuing to occur under our experimental conditions (Figures 5B–5D). Once steady-state substrate turnover had been established, we spiked reactions with buffer or a molar excess of Nas6 and then continued to measure substrate turnover. In all cases, addition of buffer or Nas6 caused a slight slowing of the substrate degradation rate compared to preaddition due to the resultant dilution of the reaction. Addition of excess Nas6 caused minimal slowing of substrate degradation for purified yeast 26S proteasomes (Figure 5B), reconstituted proteasomes containing WT lid (Figure 5C), or reconstituted proteasomes containing rpn5-s1mut lid (Figure 5D) compared to buffer addition. This indicated that Nas6 causes little to no dissociation of mature 26S proteasomes, even when the Rpn5 s1 contact is disrupted. This further supports a model in which Nas6 primarily interferes with 26S stability before RP-CP association in *rpn5-s1mut* cells.

We next directly tested whether the Rpn5 s1 mutations compromised Nas6 eviction from nascent 26S proteasomes. We immobilized *nas6Δ* yBase on FLAG beads via a 3×FLAG tag on the non-ATPase base subunit Rpn1 in the presence or absence of recombinant Nas6. After washing away any unbound Nas6, we added purified WT or s1mut lid, Rpn10, and CP. Assembly of 26S proteasomes was then monitored by retention of lid and CP on the beads by the base, and release of Nas6 was monitored by detection of Nas6 in the supernatant (Figure 5E). When Nas6 was omitted, 26S proteasomes were efficiently assembled based on retention of both lid and CP on the beads (Figure 5F, lanes 3 and 4). However, when the base was preloaded with Nas6, both WT and s1mut lid were efficiently retained, but CP retention was partially compromised in the presence of s1mut lid (Figure 5F, lanes 6 and 7). Consistent with our *in vivo* observations, the samples containing s1mut lid showed decreased release of Nas6 into the supernatant (Figure 5F, lanes 6 and 7). Altogether, these findings strongly support a model in which the Rpn5 s1 contact functions primarily by promoting eviction of Nas6 from nascent 26S proteasomes, ratherthan destabilizing mature 26S proteasomes.

ATP Binding by Rpt3 and Rpt6 Reciprocally Modulates the *rpn5-s1mut* Assembly Defect

ATP binding and hydrolysis cause conformational rearrangements within the proteasome, raising the possibility that the conformation-specific function of Rpn5 in Nas6 eviction could be linked to the nucleotide state of the base. We used the slowly hydrolyzable ATP analog ATPγS to test the impact of nucleotide binding on the *rpn5-s1mut* assembly defect.

Author Manuscript Author Manuscript Author Manuscript Author Manuscript

ATPγS is poorly hydrolyzed by proteasomal ATPases and thus promotes ATP-bound conformations (Eisele et al., 2018; Śledź et al., 2013; Zhu et al., 2018). We prepared extracts of WT or *rpn5-s1mut* cells in the presence of either ATP or ATPγS and then examined proteasome assembly state via native PAGE immunoblotting (Figure 6A; Figures S6A and S6B). The accumulation of RP and CP observed in extracts of *rpn5-s1mut* cells prepared in the presence of ATP was potently suppressed by preparation of extracts in the presence of ATPγS. This suggests that ATP binding by one or more ATPase subunits could bypass the requirement for the Rpn5 s1 contact with the base and thus act downstream of the Rpn5 s1 contact.

One possible explanation for suppression of the *rpn5-s1mut* assembly defect by ATPγS is that ATPγS allows the formation of a ternary Nas6-RP-CP complex that resembles mature 26S proteasomes by native PAGE. If so, then Nas6 should readily copurify both RP and CP subunits in the presence of ATPγS from *rpn5-s1mut* yeast. To test this, we purified Nas6-associated complexes from WT or *rpn5-s1mut* strains expressing Nas6–3×FLAG from the *NAS6* chromosomal locus. As reported previously (Roelofs et al., 2009), Nas6 failed to detectably coprecipitate CP subunits in WT cells in the presence of ATP orATPγS (Figure 6B). Similarly, no CP subunits were evident in Nas6 immunoprecipitations from *rpn5-s1mut* yeast performed in the presence of ATP. No CP subunits copurified with Nas6 from *rpn5-s1mut* cells even in the presence of ATPγS. Similar results were obtained when the CP was immunoprecipitated and assayed for copurification of Nas6 (Figure S6C). Thus, the *rpn5-s1mut* defect does not obviously allow formation of a ternary Nas6-RP-CP complex in the presence of ATPγS, and nucleotide binding by one or more ATPase subunits must therefore act downstream of the Rpn5 s1 contact during Nas6 eviction.

To distinguish the effects of individual nucleotide binding events on proteasome assembly, we introduced glutamate-to-glutamine substitutions into the conserved Walker B motifs of the proteasomal ATPases (*rpt-EQ*). These mutations prevent ATP hydrolysis by the respective Rpt subunit, thereby enriching the ATP-bound state. We have previously shown that *rpt2-EQ, rpt3-EQ*, and *rpt6-EQ* mutant yeast are viable, whereas *rpt1-EQ, rpt4-EQ*, and *rpt5-EQ* mutant yeast are not (Eisele et al., 2018), so we focused our attention on Rpt2, Rpt3, and Rpt6. We introduced each of these *rpt-EQ* mutants into *RPN5* or *rpn5-s1mut* strains and performed native PAGE immunoblotting in the presence of ATP (Figure 6C; Figure S6D-S6F). The *rpt2-EQ rpn5-s1mut* double mutant had a similar amount of free RP and CP compared to *rpn5 s1mut* alone, suggesting that ATP binding by this subunit does not affect RP-CP association. However, the RP-CP defect was absent from *rpt3-EQ rpn5-s1mut* extracts. In surprising contrast, the defect was exacerbated in the *rpt6-EQ rpn5-s1mut* double mutant, which displayed almost undetectable levels of RP_2CP. The *rpt2-EQ* and *rpt6-EQ* mutations did not affect binding of Nas6 to RP, because we readily detected Nas6-bound RP in native immunoblots (Figure S6F). Although the lack of free RP in *rpn5-s1mut rpt3-EQ* cells precluded direct analysis of Nas6 binding to RP by native PAGE, purified *rpt3-EQ* base bound Nas6 *in vitro* (data not shown). Altogether, these data indicate that the nucleotide states of Rpt3 and Rpt6 regulate Rpn5-dependent RP-CP stability. Considering that Rpt6 does not contact Nas6 or Rpn5 directly, the *rpt6-EQ* mutation must act allosterically through one of its neighboring ATPases: Rpt2 or Rpt3. Because the *rpt2-EQ* mutation had no impact on RP-CP association, Rpt6 most likely acts through Rpt3. The enhancement of the *rpn5-*

Author Manuscript Author Manuscript Author Manuscript Author Manuscript

s1mut defect in *rpt6-EQ* yeast suggests that nucleotide binding by Rpt6 negatively regulates ATP binding by Rpt3. Altogether, these data indicate an allosteric pathway in which conformation-dependent contact of Rpn5 with the base promotes nucleotide-dependent eviction of Nas6 by Rpt3.

DISCUSSION

We show that eviction of Nas6 from nascent 26S proteasomes depends on the formation of conformation-specific contacts between the lid subunit Rpn5 and the base and that Rpt3 is the major effector of this conformation-dependent eviction. These contacts are dispensable for proteasome assembly either when Nas6 is absent or when the influence of Rpn5 on Rpt3 is bypassed via provision of ATPγS or introduction of the *rpt3-EQ* mutation. These data, together with our modeling, reveal an allosteric pathway of communication between the lid and the RP-CP interface critical for efficient proteasome assembly. Our data are fully consistent with, and conceptually link, previous studies implicating Rpt3 and Rpt6 in controlling Nas6-dependent proteasome assembly (Sokolova et al., 2015), recent structures of gankyrin-bound RP (Lu et al., 2017), and the previously reported dependence of RP-CP assembly on nucleotide binding (Beckwith et al., 2013; Kim et al., 2013; Lee et al., 2012; Li et al., 2017). We posit that assembly-coupled conformational changes in other chaperone-bound ATPase subunits within the proteasome may function similarly to release their cognate bound chaperones, although whether allosteric interactions with other RP subunits are required remains unknown.

One of the most notable features of the gankyrin-bound RP compared to the RP in the context of the 26S proteasome is a large lockwasher-like split in the ATPase ring between Rpt3 and Rpt4 (Lu et al., 2017). This split is not observed in available structures of the mature 26S proteasome. In the context of the free RP, this split provides space for both Rpn5 and Nas6 or gankyrin to stably contact the base (Figure 1D). However, this split results in a highly open Rpt3 nucleotide binding pocket that likely would have a poor affinity for nucleotide due to reduced contact by Rpt4. Formation of a closed Rpt3 nucleotide binding pocket would then allow ATP binding, which in turn could promote eviction of Nas6. Our cryo-EM studies suggest that Rpt3 adopts an ATP bound-like state in s1, whereas Rpt6 assumes an empty-like state (Eisele et al., 2018). This is consistent with our findings that ATP binding by Rpt3 and Rpt6 reciprocally control RP-CP interaction (Figure 6C) and the dependence on the Rpn5 s1 contact with the base. Given that Rpn5 makes direct contact with both Rpt3 and Rpt4 in the s1 state (Unverdorben et al., 2014), we propose that Rpn5 may help to seal the ATPase ring upon association of the chaperone-bound RP with the CP (Figure 7). Such a model rationalizes the dependence on the Rpn5 s1 contact, as well as the impact of the *rpt3-EQ* mutation on Nas6-dependent proteasome assembly. One important implication for biochemical studies of proteasome biogenesis derives from most *in vitro* experiments on RP assembly having been performed with base purified by dissociating mature 26S proteasomes (Leggett et al., 2005). If assembly-coupled ring closure is irreversible and triggered by RP-CP interaction, then this purified base may not perfectly mimic the native RP assembly intermediate. This may explain a report (Li et al., 2017) that preincubation of purified, Nas6-bound base with ATPγS reduced its association with the lid, whereas preincubation with ATP reduced its association with the CP, which we have also

Author Manuscript Author Manuscript Author Manuscript Author Manuscript

observed (data not shown) and is seemingly at odds with the association of all three subcomplexes and our cell-based ATPγS experiments (Figure 6). Further structural studies will be necessary to address this possibility.

Nas6 reciprocally blocks lid-base or base-CP association in a manner dependent on the nucleotide state of the base via steric clash with Rpn6 or the CP, respectively (Li et al., 2017). How these seemingly antithetical steric conflicts are overcome to allow 26S proteasome formation has been unclear. It was proposed that the RP must cycle through both s3-like and s1-like states to allow base-CP association and base-lid association, respectively, with Nas6 release associated with the s1-like state (Li et al., 2017). The finding that gankyrin-RP assumes an open-ring state that can support formation of a ternary gankyrin-RP-CP complex without obvious steric clash between gankyrin and Rpn6 or the CP (Lu et al., 2017) may circumvent the proposed requirement for an s3-like state that is seemingly incompatible with lid-base association. Our findings that formation of the Rpn5 s1 contact is crucial for successful RP-CP association and is regulated by ATP binding by Rpt3 and Rpt6 are consistent with both studies and clarify how conformational changes complete 26S proteasome maturation. Altogether, these works indicate that Nas6 can control two distinct proteasome assembly steps (lid-base or base-CP association versus RP-CP association) via conformation-dependent clashes with two distinct lid subunits. The relative contributions of each function to CP-dependent versus CP-independent RP assembly remain to be determined.

Assembly of the RP and CP was previously linked to the interaction of the Rpt3 and Rpt6 C-terminal tails with the surface of the CP (Sokolova et al., 2015) and was proposed to trigger Nas6 eviction upon RP-CP association (Li et al., 2017). Furthermore, the *rpt3-Δ1* mutant, which cannot engage the CP effectively due to truncation of its C-terminal tail, was shown to accumulate Nas6 on mature proteasomes (Park et al., 2009). In light of these observations and our current work, we speculate that docking of the Rpt3 tail may be triggered by ATP binding to Rpt3 and that the resultant tight interaction with the CP allows for the shoehorning of Nas6 from Rpt3 in a manner dependent on the Rpn5 s1 contact. Alternatively, docking of the tail may help drive closure of the Rpt3 nucleotide pocket during assembly to allow ATP binding and subsequent Nas6 eviction. We favor the former possibility partly because *rpt3-Δ 1* yeast do not display the overt proteolytic defects that would be anticipated from a structurally defective ATPase ring (Park et al., 2009). Furthermore, our data are most consistent with Rpn5 promoting the closed, ATP-bound state of Rpt3 via its conformation-specific interaction with Rpt3-Rpt4.

Rpt3 and Rpt6 reciprocally control RP-CP stability during 26S proteasome assembly. Our data suggest that Rpt6 allosterically regulates Rpt3 ATP binding, as expected based on mechanistic studies of the archaeal proteasomal ATPase (Kim et al., 2015; Smith et al., 2011) and of related AAA+ family ATPases (Stinson et al., 2013). This can be understood if the proteasomal ATPase ring undergoes counterclockwise rotary hydrolysis, as has been proposed (de la Peña et al., 2018; Eisele et al., 2018; Kim et al., 2015). In this model, the ATP-bound subunits are trailed by ADP-bound (or potentially, empty) subunits (de la Peña et al., 2018; Eisele et al., 2018; Kim et al., 2015). If the assumption is made that introduction of an *rpt-EQ* mutation stalls the proteasome in a configuration in which the *rpt-EQ* subunit is

Author Manuscript Author Manuscript Author Manuscript Author Manuscript

the lagging ATP-bound subunit, then the *rpt3-EQ* mutation would be predicted to stall proteasomes with Rpt3 in an ATP-bound state. In contrast, the *rpt6-EQ* mutant would instead stall with Rpt3 in an ADP-bound (or empty) state. This has implications for the sequence of conformational dynamics during assembly. Because Rpt3 and Rpt6 assume ATP-bound and ADP or empty conformations in the s1 state, respectively (Eisele et al., 2018), and because Rpt6 assumes an ATP-bound conformation in all known s3-like states (Eisele et al., 2018), RP-CP docking most likely must initiate via formation of an s1-like state rather than an s3-like state. This passage first through an s1-like state, leading to Nas6 eviction, may explain the lack of an obvious assembly defect in *rpn5-s3mut* (Figure 2B), despite substantial steric clash with Nas6 (Figure 1C).

Because such conformation-coupled eviction of Nas6 depends on both formation of appropriate lid-base contacts and nucleotide binding by ATPase subunits, chaperone eviction may act as a checkpoint during assembly to ensure that only functional RP that can assume the s1 conformation will stably dock with CP to form 26S proteasomes. A structurally or functionally defective proteasome (represented in our study by the *rpn5-s1mut*) would thereby fail to eject Nas6, leading to aborted RP-CP docking, as we have observed (Figure 2B). In this way, Nas6 (and potentially the other chaperones) may protect against formation of nascent 26S proteasomes that are functionally or conformationally defective, which warrants further investigation. A similar functional and conformational checkpoint has been demonstrated for the ribosome (Ghalei et al., 2017). In this checkpoint, nascent 40S ribosomes are tested for their ability to undergo conformational changes important for protein translation, and only upon successful completion of this test do the bound assembly factors dissociate to complete maturation. Such a checkpoint-like function of Nas6 could potentially be exploited therapeutically. There is increasing interest in impairing proteasome assembly as a novel means of cancer therapy (Grigoreva et al., 2015; Izumikawaet al., 2010), and gankyrin is overexpressed in many human cancers (Fu et al., 2002; He et al., 2016; Hwang et al., 2014; Liu et al., 2014; Sakurai et al., 2017). These gankyrin-overexpressing cancers may be particularly sensitive to inhibition of proteasome assembly upon blockade of ATP binding by Rpt3.

STAR⋆METHODS

CONTACT FOR REAGENT AND RESOURCE SHARING

Further information and requests for resources and reagents should be directed to and will be fulfilled by the Lead Contact, Robert J. Tomko Jr. (robert.tomko@med.fsu.edu).

EXPERIMENTAL MODEL AND SUBJECT DETAILS

All yeast strains were grown in YPD medium at 30°C, except for *RPT* Walker B mutants and their derivatives, which were grown at 25°C. When selection for a plasmid was necessary, strains were grown in synthetic dropout medium lacking the appropriate auxotrophic agent at 30°C or 25°C as above.

Author Manuscript Author Manuscript Author Manuscript Author Manuscript

METHOD DETAILS

Yeast strains and media—All yeast manipulations were carried out according to standard protocols (Guthrie and Fink, 1991). Yeast strains used in this study are listed in Table S1. We created yeast strains with chromosomal deletions of *RPN5* or *SCL1* (α1) covered by a URA3-marked plasmid bearing the corresponding WT allele. Single mutant strains were crossed, and double mutants were isolated after sporulation and dissection. Double mutants were identified via growth on selective media and/or colony PCR. WT or mutant proteasome subunit alleles on *LEU2*- or TRP1-marked plasmids (Mumberg et al., 1995) were then introduced into the double mutant strain, and the URA3-marked plasmids were evicted by selection on 5-fluoroorotic acid media. For growth assays, the indicated strains were spotted as six-fold serial dilutions in water onto the indicated media.

Plasmids—All plasmids were constructed using standard molecular cloning techniques using TOP10 F' (Invitrogen) as a host strain. QuikChange (Agilent) was used for site-directed mutagenesis and the resultant plasmids were sequenced prior to use. Plasmids used in this study are listed in Table S2.

Molecular modeling and measurement of clash—The structure of the Rpt3 C-terminal domain (as part of a Nas6-Rpt3 complex, PDB: 2ZDN) was aligned with Rpt3 over residues 350–410 in the s1 (PDB: 4CR2), s2 (PDB: 4CR3), s3 (PDB: 4CR4), s4 (PDB: 5MCP), s5 (PDB: 6FVX), and s6 (PDB: 6FVY) conformations of the yeast proteasome using Pymol. RMSD over all backbone atoms was ≤ 2 Å in each case. Steric clash was identified by visual inspection in space-filling mode. The Nas6-Rpt3 crystal structure contains three protomers in the asymmetric unit; the clashes reported were observed when any of the protomers were used for alignment.

For measurement of steric clash, structures were first superimposed via alignment of Rpt3-C domains using the Matchmaker command in UCSF Chimera (Pettersen et al., 2004). Steric clash was then measured via the Find Clashes/Contacts command using Nas6 as the reference chain against either full-length Rpn5 or the full CP α ring. The minimum van der Waals overlap was set to 2.0 Å to account for ambiguity in the EM model based on the above finding that RMSD for Rpt3-C alignment was ≤ 2Å.

Non-denaturing polyacrylamide gel electrophoresis—For analysis of cell extracts, 60 μg of total protein was separated by 4% non-denaturing PAGE as described previously (Nemec et al., 2017). Specifically, cells were grown to OD_{600} ≈ 2.0, harvested by centrifugation at 8,000 × g for five minutes at RT, followed by washing in 25 mLof ice-cold dH_2O. Cells were centrifuged again at 5,000 × g for two minutes, 4°C, and the supernatant was poured off. Cell pellets were then frozen in liquid nitrogen and ground into powder using a mortar and pestle. Cell powder was hydrated in one powder volume of extraction buffer (50 mM Tris-Cl, pH 7.5, 5 mM $MgCl_2$,10% glycerol, 1 mM ATP, 0.015% w/v xylene cyanol), and incubated with frequent vortexing for 10 minutes on ice. In some experiments, ATP was replaced with ATPgS. Cell debris was removed by centrifugation at 21,000 × g for 10 minutes at 4°C. Supernatants containing equal amounts of protein (determined by BCA assay) were loaded onto 4% native polyacrylamide gels cast with 0.5 mM ATP and with a

Author Manuscript Author Manuscript Author Manuscript Author Manuscript

3.5% polyacrylamide stacker containing 2.5% sucrose and 0.5 mM ATP. Samples were electrophoresed at 100 V, 4°C until the dye front escaped.

Immunoblot analyses—Proteins separated by native PAGE or SDS-PAGE were transferred to PVDF membranes and immunoblotted with antibodies against Rpn12 (1:5000), 20S (1:2500), Rpt1 (1:10,000), FLAG (1:5000), β-actin (1:5000), ubiquitin (1:1000), V5 (1:5000), G6PD (1:20,000), Rpt5 (1:10,000), Rpn14 (1:5000), Nas2 (1:5000), Hsm3 (1:5000), or Nas6 (1:10,000). Blots were imaged on a Bio-Rad ChemiDoc MP using HRP-conjugated secondary antibodies (GE Healthcare) and ECL reagent.

Purification of nas6Δ base from yeast—Base lacking Nas6 was isolated from strain RTY2078 via FLAG affinity, followed by gel filtration to remove contaminating assembly intermediates. Six liters of YPD inoculated with RTY2078 was grown until saturation, followed by harvesting at 8000 × g for 5 minutes, 4°C. The cell pellet was washed once in 250 mL of dH_2O, and snap-frozen in liquid nitrogen. The frozen cells were then ground into powder using a SPEX6850 freezer mill, and stored at −80°C. The day of purification, the cell powder was thawed in an equal volume of yBase Buffer (50 mM HEPES-OH, pH 7.5, 50 mM NaCl, 50 mM KCl, 5 mM $MgCl_2$, 0.5 mM EDTA, 10% glycerol) supplemented with 500 μM ATP and 0.05% NP-40 and stirred until thawed. The insoluble debris was pelleted at 30,000 × g for 20 minutes, 4°C, and the supernatant was added to FLAG M2 agarose and allowed to mix for 90 minutes. The resin was collected at 1500 × g for two minutes, 4°C, and the supernatant was decanted. The resin was then washed three times in yBase buffer containing ATP but not NP-40, followed by elution via incubation with 200 μg/mL 3×FLAG peptide for 45 minutes at 4°C. The eluted complexes were then concentrated in a 30,000 Da MWCO filter (Amicon), and further purified by gel filtration on a Superose 6 10–30 column in yBase Buffer supplemented with 500 μM ATP. Pure fractions were pooled, concentrated as above, snap-frozen in liquid nitrogen, and stored at − 80° C in small aliquots.

Purification of CP from yeast—CP was purified from strain RTY366 (Sá-Moura et al., 2013) essentially as described for the *nas6Δ* base, but with the following exceptions: 1) CP Buffer (50 mM Tris·Cl, pH 7.5, 50 mM NaCl, 50 mM KCl, 0.5 mM EDTA) lacking ATP and containing 0.05% NP-40 was used for protein extraction; 2) the FLAG resin was washed with CP Wash Buffer (50 mM Tris·Cl, pH 7.5,500 mM NaCl, 0.5 mM EDTA, 0.05% NP-40) instead of yBase buffer; and 3) gel filtration was performed in CP Buffer.

Purification of recombinant Nas6, Rpn14, and Ub_4-GFP-Tail—Nas6, Rpn14, and Ub_4-GFP-Tail were expressed as C-terminal 6His fusions from plasmids pRT37, pRT39, and pRT1887, respectively, in bacterial strain LOBSTR (DE3) cotransformed with pRARE2. Transformants were grown in 2 L of LB and the appropriate antibiotics at 37°C, 250 rpm shaking until OD_{600} = 0.6, at which point the temperature was reduced to 16°C and IPTG was added to 0.5 mM. After overnight induction, cultures were centrifuged at 8000 × g for 5 minutes, 4°C, the supernatant was poured off, and cells were frozen at −80°C until purification. The day of purification, cells were thawed in NPI-10 (10 mM sodium phosphate, pH 8.0, 300 mM NaCl, 10 mM imidazole), and lysed with an Avestin Emulsiflex C-5. Lysates were clarified via centrifugation at 30,000 × g for 20 minutes, 4°C, and the

Author Manuscript Author Manuscript Author Manuscript Author Manuscript

supernatant was incubated with Ni-NTA resin for 30 minutes at 4°C. After two washes with NPI-10, the resin was poured into a disposable Bio-Rad Econo-column, washed with NPI-20 (10 mM sodium phosphate, pH 8.0, 300 mM NaCl, 20 mM imidazole), and eluted with NPI-500 (10 mM sodium phosphate, pH 8.0, 100 mM NaCl, 500 mM imidazole). Eluates were concentrated using 10,000 Da MWCO filters (Amicon), and further purified by gel filtration on a Sephacryl S-200 column in Lid Buffer (50 mM HEPES·OH, pH 7.5, 100 mM NaCl, 100 mM KCl, 5% glycerol). Pure fractions were pooled, concentrated as above, and snap-frozen as small aliquots in liquid nitrogen for storage at −80°C.

Purification of recombinant Rpn10—Rpn10 was expressed from pRT205 as an N-terminal 6His fusion in bacterial strain LOBSTR (DE3) cotransformed with pRARE2. Transformants were grown in 2 L of LB and the appropriate antibiotics at 37°C, 250 rpm shaking until OD_{600} = 0.6, at which point the temperature was reduced to 30°C and IPTG was added to 0.5 mM. After four hours, cultures were centrifuged at 8000 × g for 5 minutes, 4°C, the supernatant was poured off, and cells were frozen at −80°C until purification. The day of purification, cells were thawed in Buffer A (50 mM tris·Cl, pH 7.5, 150 mM NaCl, 5 mM $MgCl_2$, 10% glycerol) supplemented with 20 mM imidazole, and lysed with an Avestin Emulsiflex C-5. Lysates were clarified via centrifugation at 30,000 × g for 20 minutes, 4°C, and the supernatant was incubated with Ni-NTA resin for 30 minutes at 4°C. After two washes with Buffer A containing 20 mM imidazole, the resin was poured into a disposable Bio-Rad Econo-column, washed again, and eluted with Buffer A containing 500 mM imidazole. Eluates were concentrated using 10,000 Da MWCO filters (Amicon), and further purified by gel filtration on a Sephacryl S-200 column in Buffer A. Pure fractions were pooled, concentrated as above, and snap-frozen as small aliquots in liquid nitrogen for storage at −80°C.

Purification of recombinant lid complexes—Fully recombinant lid complex and the s1mut lid were expressed either with N-terminal 6His-FLAG tags on Rpn6 from plasmids pRT972 and pRT1609 (WT lid) or pRT1776 (s1mut-lid), or as N-terminal MBP-3Cx fusions to Rpn6 from plasmids pRT972 and pRT945 (WT lid) or pRT2100 (s1mut-lid). All forms of the lid were expressed in LOBSTR (DE3) cotransformed with pRARE2. Transformants were grown in 2 L of terrific broth and the appropriate antibiotics at 37°C until OD_{600} = 1.0, at which point the temperature was reduced to 16°C and IPTG was added to 0.5 mM. After overnight induction, cultures were centrifuged at 8000 × g for 5 minutes, 4°C, the supernatant was poured off, and cells were immediately processed for purification.

For6His-FLAG-tagged WT and mutant lid, the cells were resuspended in Lid Buffer supplemented with 5 mM β-mercaptoethanol, 20 mM imidazole, and 1 mM PMSF, and lysed with an Avestin Emulsiflex C-5. Lysates were clarified via centrifugation at 30,000 × g for 20 minutes, 4°C, and the supernatant was incubated with Ni-NTA resin for 30 minutes at 4°C. After two washes with Lid Buffer supplemented with 5 mM β-mercaptoethanol and 20 mM imidazole, the resin was poured into a disposable Bio-Rad Econo-column, washed again, and eluted with Lid Buffer supplemented with 500 mM imidazole. Eluates were concentrated using 100,000 Da MWCO filters (Amicon), and further purified by gel filtration on a Superose 6 10–30 column equilibrated in Lid Buffer. Pure fractions were

Author Manuscript Author Manuscript Author Manuscript Author Manuscript

pooled, concentrated as above, and snap-frozen as small aliquots in liquid nitrogen for storage at −80°C.

For MBP-tagged WT and mutant lid, the cells were resuspended in Lid Buffer supplemented with 1 mM DTT and 1 mM PMSF, and were lysed and clarified as above. The supernatant was then incubated with amylose resin for 30 minutes at 4°C. After two washes with Lid Buffer supplemented with 1 mM DTT, the resin was poured into a disposable Bio-Rad Econo-column, washed again, and eluted with Lid Buffer containing 20 mM D-maltose. The MBP tag was cleaved from the eluted complexes overnight at 4°C via addition of 10 mM DTT and a 1:20 (w/w) amount of HRV-3C protease, and the cleaved tag and protease were separated via gel filtration on a Superose 6 10–30 column equilibrated in Lid Buffer. Pure fractions were pooled, concentrated as above, and snap-frozen as small aliquots in liquid nitrogen for storage at −80°C.

Mass spectrometric analysis—Proteasomes were purified from *rpn5Δ* cells expressing *rpn5 s1mut-3×FLAG* from a plasmid. The RP* band was excised from native PAGE gels, and submitted to the FSU-COM Translational Science Laboratory for in-gel trypsinization and analysis by LC-MS/MS.

***In vitro* assembly assays—**Purified proteins were mixed at final concentrations of 20 nM CP, 40 nM lid or base, 200 nM Rpn10, and 1 mM Nas6 or Rpn14 and incubated at 30°C for indicated times in extraction buffer (50 mM Tris-HCl, pH 7.5, 5 mM $MgCl_2$, 10% glycerol, 0.5 mM ATP). Reactions were cooled on ice and 15 μL of samples were separated by native PAGE for immunoblotting. For Figure S4E, the concentrations were 100 nM CP, 200 nM lid or base, 200 nM Rpn10, and 1 μM Nas6.

Multiple turnover degradation assays—Degradation assays were conducted at 30°C in 26S Buffer (50 mM Tris·Cl, pH 7.5, 50 mM NaCl, 50 mM KCl, 5 mM $MgCl_2$, 1 mM EDTA, 10% glycerol, 1 mM DTT) with an ATP-regenerating system (60 μg/mL creatine kinase, 16 mM creatine phosphate, 5 mM ATP). Proteasomes were reconstituted from 100 nM purified CP, 200 nM yBase, 200 nM recombinant Rpn10, and 1 μM recombinant WT or rpn5 s1mut lid. Degradation assays were initiated by addition of 2 μM Ub_4-GFP-Tail, and degradation was monitored by the loss of GFP fluorescence (ex 479 nm, em 520 nm) on a BioTek Synergy H1MF. After 900 s, the instrument was paused, either buffer or 1 μM recombinant Nas6 was added, and degradation was monitored for another 900 s. The degradation rate remained linear for greater than 2400 s under these conditions, indicating that multiple turnover conditions were maintained for the duration of the assay.

Peptidase stimulation assays—Analysis of suc-LLVY-AMC hydrolysis by reconstituted WT or s1-mut lid-containing 26S proteasomes was conducted in the absence of Nas6 in 384-well black microplates on a Biotek Synergy H1MF. Proteasomes were reconstituted from 10 nM purified CP, 40 nM purified *nas6Δ* yBase, 40 nM WT or s1-mut lid, and 40 nM recombinant Rpn10 for 15 minutes at 30°C in 26S Buffer with ATP-regenerating system (50 mM HEPES-OH, pH 7.5, 50 mM NaCl, 50 mM KCl, 5 mM $MgCl_2$, 10% glycerol, 0.5 mM ATP, 60 μg/mL creatine kinase, and 16 mM creatine phosphate), at which point 50 mM suc-LLVY-AMC was added. Fluorescence from liberated AMC (ex 360

Author Manuscript Author Manuscript Author Manuscript Author Manuscript

nm, em 460 nm) was monitored for 900 s. Relative rates were determined from the initial slopes of fluorescence versus time, and plotted as percent of CP alone.

Co-immunopreciptiations—Immunoprecipitations were performed as previously described (Tomko et al., 2010), except 3 mg of total protein was used per sample. Yeast cell extracts were prepared as described for native PAGE analysis, except that the cell powder was thawed in Buffer A supplemented with 500 μM ATP or ATPγS. Extracts were centrifuged for 10 minutes at 21,000 × g to remove cell debris. After determining protein concentration, normalized samples were incubated with 50 μL of FLAG-M2 agarose for 90 minutes at 4°C, washed three times with ice-cold Buffer A containing 500 μM ATP or ATPγS, and bound proteins were eluted with 200 μg/mL 3×FLAG peptide for 45 minutes at 4°C. Eluates were analyzed by immunoblotting as described above.

Nas6 eviction assays—200 nM purified *nas6Δ* yBase was pre-incubated or not with 200 nM purified Nas6 for 15 minutes at 30°C in extraction buffer containing 0.5 mM ATP. The mixture was then added to 20 mL of anti-FLAG M2 agarose (Sigma) for one hour at 4°C. The beads were then washed twice with extraction buffer containing 0.5 mM ATP, and 200 nM WT or s1mut lid, 200 nM Rpn10, and 100 nM CP were added. The mixture was then incubated at 30°C for 15 minutes, and the beads were pelleted at 1200 × g for one minute, 4°C. An aliquot of the supernatant was collected to assess Nas6 release. The beads were then washed 1× in extraction buffer containing 0.5 mM ATP to remove any residual unbound proteins trapped in the resin, pelleted again, and boiled in Laemmli buffer to elute bound proteins.

Conformation-selective engineered disulfide crosslinking—Yeast expressing proteins with the desired cysteine substitutions were grown to mid-log phase, and 20 OD_{600} equivalents were harvested and converted to spheroplasts. These were lysed in 150 μL of ice-cold lysis buffer (50mM HEPES, pH 7.5,150mM NaCl, 5mM $MgCl_2$) containing 2mM nucleotide (ATP or AMP-PNP). The cells were lysed by vortexing three times at top speed for 30 s with 1 min intervals on ice in between. The lysates were centrifuged at 21,000 × g at 4°C for 10 min. The protein content of supernatants was normalized with lysis buffer containing the appropriate nucleotide. Crosslinking was initiated with 25μM $CuCl_2$ at 25°C. After 10 minutes, *N*-ethylmaleimide was added to 10 mM and EDTA was added to 10 mM final concentration to halt additional crosslinking. Samples were boiled in non-reducing Laemmli buffer, loaded onto 10% SDS-PAGE gels, and separated by electrophoresis at 200 V before immunoblotting with antibodies against V5 or G6PD as a control.

QUANTIFICATION AND STATISTICAL ANALYSIS

All experiments were performed at least twice, with most experiments being repeated three or more times. Statistical analysis was carried out using Graph Pad Prism 7.0 software using a one-way ANOVA with Tukey's test for multiple comparisons (Figure S3C). Statistical significance was considered $p < 0.05$. Exact values of *N* for each experiment can be found in the figure legends.

Author Manuscript Author Manuscript Author Manuscript Author Manuscript

Supplementary Material

Refer to Web version on PubMed Central for supplementary material.

ACKNOWLEDGMENTS

The authorsthank Mark Hochstrasser, William P. Tansey, and Andreas Matouschek for strains and reagents; the Florida State University College of Medicine Translational Science Laboratory for mass spectrometry service; Beth Stroupe for advice on quantifying steric clash; and the Florida State University yeast community for helpful discussions. This work was supported by start-up funds from Florida State University College of Medicine and NIH grant 1R01GM118600 (to R.J.T.).

REFERENCES

Bard JAM, Goodall EA, Greene ER, Jonsson E, Dong KC, and Martin A (2018). Structure and function of the 26S proteasome. Annu. Rev. Biochem 87, 697–724. [PubMed: 29652515]

Barrault MB, Richet N, Godard C, Murciano B, LeTallec B, Rousseau E, Legrand P, Charbonnier JB, Le Du MH, Guerois R, et al. (2012). Dual functions of the Hsm3 protein in chaperoning and scaffolding regulatory particle subunits during the proteasome assembly. Proc. Natl. Acad. Sci. USA 109, E1001–E1010. [PubMed: 22460800]

Beckwith R, Estrin E, Worden EJ, and Martin A (2013). Reconstitution of the 26S proteasome reveals functional asymmetries in its AAA+ unfoldase. Nat. Struct. Mol. Biol 20, 1164–1172. [PubMed: 24013205]

Chen P, Johnson P, Sommer T, Jentsch S, and Hochstrasser M (1993). Multiple ubiquitin-conjugating enzymes participate in the in vivo degradation of the yeast MAT alpha 2 repressor. Cell 74, 357–369. [PubMed: 8393731]

Chen S, Wu J, Lu Y, Ma YB, Lee BH, Yu Z, Ouyang Q, Finley DJ, Kirschner MW, and Mao Y (2016). Structural basis for dynamic regulation of the human 26S proteasome. Proc. Natl. Acad. Sci. USA 113,12991–12996. [PubMed: 27791164]

Dambacher CM, Worden EJ, Herzik MA, Martin A, and Lander GC (2016). Atomic structure of the 26S proteasome lid reveals the mechanism of deubiquitinase inhibition. eLife 5, e13027. [PubMed: 26744777]

de la Peña AH, Goodall EA, Gates SN, Lander GC, and Martin A (2018). Substrate-engaged 26S proteasome structures reveal mechanisms for ATP-hydrolysis-driven translocation. Science 362, eaav0725. [PubMed: 30309908]

Eisele MR, Reed RG, Rudack T, Schweitzer A, Beck F, Nagy I, Pfeifer G, Plitzko JM, Baumeister W, Tomko RJ, Jr., et al. (2018). Expanded Coverage of the 26S Proteasome Conformational Landscape Reveals Mechanisms of Peptidase Gating. Cell Rep 24, 1301–1315. [PubMed: 30067984]

Fu XY, Wang HY, Tan L, Liu SQ, Cao HF, and Wu MC (2002). Over-expression of p28/gankyrin in human hepatocellular carcinoma and its clinical significance. World J. Gastroenterol 8, 638–643. [PubMed: 12174370]

Funakoshi M, Tomko RJ, Jr., Kobayashi H, and Hochstrasser M (2009). Multiple assembly chaperones govern biogenesis of the proteasome regulatory particle base. Cell 137, 887–899. [PubMed: 19446322]

Geng F, and Tansey WP (2012). Similar temporal and spatial recruitment of native 19S and 20S proteasome subunits to transcriptionally active chromatin. Proc. Natl. Acad. Sci. USA 109, 6060–6065. [PubMed: 22474342]

Ghalei H, Trepreau J, Collins JC, Bhaskaran H, Strunk BS, and Karbstein K (2017). The ATPase Fap7 Tests the Ability to Carry Out Translocation-like Conformational Changes and Releases Dim1 during 40S Ribosome Maturation. Mol. Cell 67, 990–1000. [PubMed: 28890337]

Grigoreva TA, Tribulovich VG, Garabadzhiu AV, Melino G, and Barlev NA (2015). The 26S proteasome is a multifaceted target for anti-cancer therapies. Oncotarget 6, 24733–24749. [PubMed: 26295307]

Author Manuscript Author Manuscript Author Manuscript Author Manuscript

Guo Q, Lehmer C, Martinez-Sanchez A, Rudack T, Beck F, Hartmann H, Pérez-Berlanga M, Frottin F, Hipp MS, Hartl FU, et al. (2018). In Situ Structure of Neuronal C9orf72 Poly-GA Aggregates Reveals Proteasome Recruitment. Cell 172, 696–705. [PubMed: 29398115]

Guthrie C, and Fink GR (1991). Guide to Yeast Genetics and Molecular Biology (Academic Press).

Hanssum A, Zhong Z, Rousseau A, Krzyzosiak A, Sigurdardottir A, and Bertolotti A (2014). An inducible chaperone adapts proteasome assembly to stress. Mol. Cell 55, 566–577. [PubMed: 25042801]

He F, Chen H, Yang P, Wu Q, Zhang T, Wang C, Wei J, Chen Z, Hu H, Li W, and Cao J (2016). Gankyrin sustains PI3K/GSK-3β/β-catenin signal activation and promotes colorectal cancer aggressiveness and progression. Oncotarget 7, 81156–81171. [PubMed: 27835604]

Howell LA, Tomko RJ, and Kusmierczyk AR (2017). Putting it all together: intrinsic and extrinsic mechanisms governing proteasome biogenesis. Front. Biol 12, 19–48.

Huang X, Luan B, Wu J, and Shi Y (2016). An atomic structure of the human 26S proteasome. Nat. Struct. Mol. Biol 23, 778–785. [PubMed: 27428775]

Hwang JA, Yang HM, Hong DP, Joo SY, Choi YL, Park JH, Lazar AJ, Pollock RE, Lev D, and Kim SJ (2014). Gankyrin is a predictive and oncogenic factor in well-differentiated and dedifferentiated liposarcoma. Oncotarget 5, 9065–9078. [PubMed: 25238053]

Izumikawa M, Hashimoto J, Hirokawa T, Sugimoto S, Kato T, Takagi M, and Shin-Ya K (2010). JBIR-22, an inhibitor for protein-protein interaction of the homodimer of proteasome assembly factor 3. J. Nat. Prod 73,628–631. [PubMed: 20180542]

Kaneko T, Hamazaki J, Iemura S, Sasaki K, Furuyama K, Natsume T, Tanaka K, and Murata S (2009). Assembly pathway of the mammalian proteasome base subcomplex is mediated by multiple specific chaperones. Cell 137, 914–925. [PubMed: 19490896]

Kim YC, Li X, Thompson D, and DeMartino GN (2013). ATP binding by proteasomal ATPases regulates cellular assembly and substrate-induced functions of the 26 S proteasome. J. Biol. Chem 288, 3334–3345. [PubMed: 23212908]

Kim YC, Snoberger A, Schupp J, and Smith DM (2015). ATP binding to neighbouring subunits and intersubunit allosteric coupling underlie proteasomal ATPase function. Nat. Commun 6, 8520. [PubMed: 26465836]

Kock M, Nunes MM, Hemann M, Kube S, Dohmen RJ, Herzog F, Ramos PC, and Wendler P (2015). Proteasome assembly from 15S precursors involves major conformational changes and recycling of the Pba1-Pba2 chaperone. Nat. Commun 6, 6123. [PubMed: 25609009]

Kriegenburg F, Seeger M, Saeki Y, Tanaka K, Lauridsen AM, Hartmann-Petersen R, and Hendil KB (2008). Mammalian 26S proteasomes remain intact during protein degradation. Cell 135, 355–365. [PubMed: 18957208]

Kusmierczyk AR, Kunjappu MJ, Funakoshi M, and Hochstrasser M (2008). A multimeric assembly factor controls the formation of alternative 20S proteasomes. Nat. Struct. Mol. Biol 15, 237–244. [PubMed: 18278055]

Le Tallec B, Barrault MB, Guérois R, Carré T, and Peyroche A (2009). Hsm3/S5b participates in the assembly pathway of the 19S regulatory particle of the proteasome. Mol. Cell 33, 389–399. [PubMed: 19217412]

Lee SH, Moon JH, Yoon SK, and Yoon JB (2012). Stable incorporation of ATPase subunits into 19Sregulatory particle of human proteasome requires nucleotide binding and C-terminal tails. J. Biol. Chem 287, 9269–9279. [PubMed: 22275368]

Leggett DS, Glickman MH, and Finley D (2005). Purification of proteasomes, proteasome subcomplexes, and proteasome-associated proteins from budding yeast. Methods Mol. Biol 301, 57–70. [PubMed: 15917626]

Li F, Tian G, Langager D, Sokolova V, Finley D, and Park S (2017). Nucleotide-dependent switch in proteasome assembly mediated by the Nas6 chaperone. Proc. Natl. Acad. Sci. USA 114, 1548–1553. [PubMed: 28137839]

Liu Y, Zhang J, Qian W, Dong Y, Yang Y, Liu Z, Feng Y, Ma D, Zhang Z, and Wu S (2014). Gankyrin is frequently overexpressed in cervical high grade disease and is associated with cervical carcinogenesis and metastasis. PLoS ONE 9, e95043. [PubMed: 24751719]

Author Manuscript Author Manuscript Author Manuscript Author Manuscript

Lu Y, Wu J, Dong Y, Chen S, Sun S, Ma YB, Ouyang Q, Finley D, Kirschner MW, and Mao Y (2017). Conformational Landscape ofthe p28-Bound Human Proteasome Regulatory Particle. Mol. Cell 67, 322–333. [PubMed: 28689658]

Luan B, Huang X, Wu J, Mei Z, Wang Y, Xue X, Yan C, Wang J, Finley DJ, Shi Y, and Wang F (2016). Structure of an endogenous yeast 26S proteasome reveals two major conformational states. Proc. Natl. Acad. Sci. USA 113, 2642–2647. [PubMed: 26929360]

Matyskiela ME, Lander GC, and Martin A (2013). Conformational switching of the 26S proteasome enables substrate degradation. Nat. Struct. Mol. Biol 20, 781–788. [PubMed: 23770819]

Mumberg D, Müller R, and Funk M (1995). Yeast vectors for the controlled expression of heterologous proteins in different genetic backgrounds. Gene 156, 119–122. [PubMed: 7737504]

Nakamura Y, Umehara T, Tanaka A, Horikoshi M, Padmanabhan B, and Yokoyama S (2007). Structural basis for the recognition between the regulatory particles Nas6 and Rpt3 of the yeast 26S proteasome. Biochem. Biophys. Res. Commun 359, 503–509. [PubMed: 17555716]

Nemec AA, Howell LA, Peterson AK, Murray MA, and Tomko RJ, Jr. (2017). Autophagic clearance of proteasomes in yeast requires the conserved sorting nexin Snx4. J. Biol. Chem 292, 21466–21480. [PubMed: 29109144]

Park S, Roelofs J, Kim W, Robert J, Schmidt M, Gygi SP, and Finley D (2009). Hexameric assembly of the proteasomal ATPases is templated through their C termini. Nature 459, 866–870. [PubMed: 19412160]

Park S, Li X, Kim HM, Singh CR, Tian G, Hoyt MA, Lovell S, Battaile KP, Zolkiewski M, Coffino P, et al. (2013). Reconfiguration of the proteasome during chaperone-mediated assembly. Nature 497, 512–516. [PubMed: 23644457]

Pettersen EF, Goddard TD, Huang CC, Couch GS, Greenblatt DM, Meng EC, and Ferrin TE (2004). UCSF Chimera—a visualization system for exploratory research and analysis. J. Comput. Chem 25, 1605–1612. [PubMed: 15264254]

Roelofs J, Park S, Haas W, Tian G, McAllister FE, Huo Y, Lee BH, Zhang F, Shi Y, Gygi SP, and Finley D (2009). Chaperone-mediated pathway of proteasome regulatory particle assembly. Nature 459, 861–865. [PubMed: 19412159]

Sá-Moura B, Funakoshi M, Tomko RJ, Jr., Dohmen RJ, Wu Z, Peng J, and Hochstrasser M (2013). A conserved protein with AN1 zinc finger and ubiquitin-like domains modulates Cdc48 (p97) function in the ubiquitin-proteasome pathway. J. Biol. Chem 288, 33682–33696. [PubMed: 24121501]

Saeki Y, Toh -EA, Kudo T, Kawamura H, and Tanaka K (2009). Multiple proteasome-interacting proteins assist the assembly of the yeast 19S regulatory particle. Cell 137, 900–913. [PubMed: 19446323]

Sakurai T, Higashitsuji H, Kashida H, Watanabe T, Komeda Y, Nagai T, Hagiwara S, Kitano M, Nishida N, Abe T, et al. (2017). The oncoprotein gankyrin promotes the development of colitis-associated cancer through activation of STAT3. Oncotarget 8, 24762–24776. [PubMed: 28160571]

Satoh T, Saeki Y, Hiromoto T, Wang YH, Uekusa Y, Yagi H, Yoshihara H, Yagi-Utsumi M, Mizushima T, Tanaka K, and Kato K (2014). Structural basis for proteasome formation controlled by an assembly chaperone nas2. Structure 22, 731–743. [PubMed: 24685148]

Schmidt M, and Finley D (2014). Regulation of proteasome activity in health and disease. Biochim. Biophys. Acta 1843, 13–25. [PubMed: 23994620]

Śledź P, Unverdorben P, Beck F, Pfeifer G, Schweitzer A, Förster F, and Baumeister W (2013). Structure of the 26S proteasome with ATP-γS bound provides insights into the mechanism of nucleotide-dependent substrate translocation. Proc. Natl. Acad. Sci. USA 110, 7264–7269. [PubMed: 23589842]

Smith DM, Chang SC, Park S, Finley D, Cheng Y, and Goldberg AL (2007). Docking of the proteasomal ATPases' carboxyl termini in the 20S proteasome's alpha ring opens the gate for substrate entry. Mol. Cell 27,731–744. [PubMed: 17803938]

Smith DM, Fraga H, Reis C, Kafri G, and Goldberg AL (2011).ATP binds to proteasomal ATPases in pairs with distinct functional effects, implying an ordered reaction cycle. Cell 144, 526–538. [PubMed: 21335235]

Author Manuscript Author Manuscript Author Manuscript Author Manuscript

Sokolova V, Li F, Polovin G, and Park S (2015). Proteasome Activation is Mediated via a Functional Switch of the Rpt6 C-terminal Tail Following Chaperone-dependent Assembly. Sci. Rep 5, 14909. [PubMed: 26449534]

Stinson BM, Nager AR, Glynn SE, Schmitz KR, Baker TA, and Sauer RT (2013). Nucleotide binding and conformational switching in the hexameric ring of a AAA+ machine. Cell 153, 628–639. [PubMed: 23622246]

Tomko RJ, Jr., and Hochstrasser M (2011). Order of the proteasomal ATPases and eukaryotic proteasome assembly. Cell Biochem. Biophys 60, 13–20. [PubMed: 21461838]

Tomko RJ, Jr., and Hochstrasser M (2013). Molecular architecture and assembly of the eukaryotic proteasome. Annu. Rev. Biochem 82, 415–445. [PubMed: 23495936]

Tomko RJ, Jr., and Hochstrasser M (2014). The intrinsically disordered Sem1 protein functions as a molecular tether during proteasome lid biogenesis. Mol. Cell 53, 433–443. [PubMed: 24412063]

Tomko RJ, Jr., Funakoshi M, Schneider K, Wang J, and Hochstrasser M (2010). Heterohexameric ring arrangement of the eukaryotic proteasomal ATPases: implications for proteasome structure and assembly. Mol. Cell 38, 393–403. [PubMed: 20471945]

Tomko RJ, Jr., Taylor DW, Chen ZA, Wang HW, Rappsilber J, and Hochstrasser M (2015). A Single α Helix Drives Extensive Remodeling of the Proteasome Lid and Completion of Regulatory Particle Assembly. Cell 163, 432–44. [PubMed: 26451487]

Unverdorben P, Beck F, Śledź P, Schweitzer A, Pfeifer G, Plitzko JM, Baumeister W, and Förster F (2014). Deep classification of a large cryo-EM dataset defines the conformational landscape of the 26S proteasome. Proc. Natl. Acad. Sci. USA 111, 5544–5549. [PubMed: 24706844]

Wani PS, Rowland MA, Ondracek A, Deeds EJ, and Roelofs J (2015). Maturation of the proteasome core particle induces an affinity switch that controls regulatory particle association. Nat. Commun 6, 6384. [PubMed: 25812915]

Wehmer M, Rudack T, Beck F, Aufderheide A, Pfeifer G, Plitzko JM, Förster F, Schulten K, Baumeister W, and Sakata E (2017). Structural insights into the functional cycle of the ATPase module of the 26S proteasome. Proc. Natl. Acad. Sci. USA 114, 1305–1310. [PubMed: 28115689]

Zhu Y, Wang WL, Yu D, Ouyang Q, Lu Y, and Mao Y (2018). Structural mechanism for nucleotide-driven remodeling of the AAA-ATPase unfoldase in the activated human 26S proteasome. Nat. Commun 9, 1360. [PubMed: 29636472]

Author Manuscript Author Manuscript Author Manuscript Author Manuscript

Highlights

- Mechanism of assembly-coupled Nas6 chaperone eviction from nascent 26S proteasomes
- Conformation-specific release of Nas6 is triggered by steric clash
- Nucleotide state of ATPase subunits Rpt3 and Rpt6 conveys eviction signal
- Nas6 may protect against assembly of structurally defective 26S proteasomes

Author Manuscript Author Manuscript Author Manuscript Author Manuscript

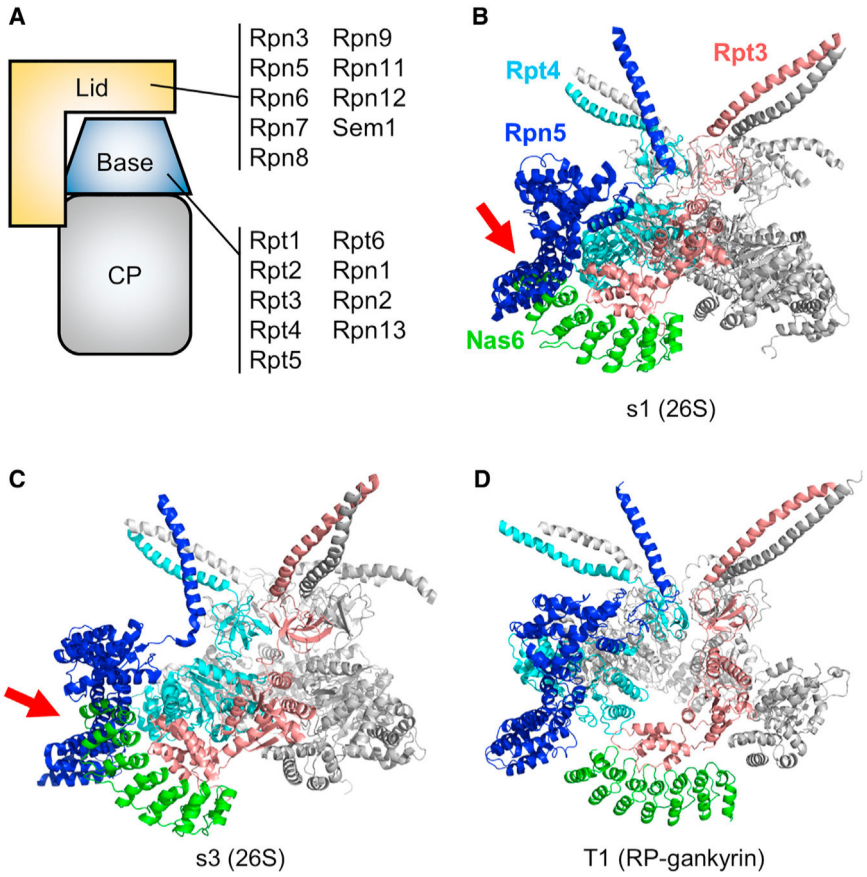

Figure 1. Prominent Steric Clash between Rpn5 and Nas6 in the s1 and s3 26S Proteasome Conformations

(A) Illustration of the 26S proteasome. The composition of the lid and base subcomplexes is shown.

(Band C) Atomic structure of Nas6 in complex with the C-terminal domain of Rpt3 (PDB: 2DZN) was modeled onto a pseudoatomic model of the 26S proteasome s1 state (PDB: 4CR2) (B) or the s3 state (PDB: 4CR4) (C) by superimposing the Rpt3 C-terminal domains in Pymol. The red arrows indicate the steric clash between Rpn5 (dark blue) and Nas6 (green) in both the s1 and the s3 states. Rpt3 is shown in salmon, and Rpt4 is shown in cyan..

(D) There is no obvious steric clash in the structure of the human RP bound by the Nas6 ortholog gankyrin (PDB: 5VHF)..

Coloring in (C) and (D) is as in (B). Many subunits are omitted for clarity..

See also Figure S1 and Table S3.

Author Manuscript Author Manuscript Author Manuscript Author Manuscript

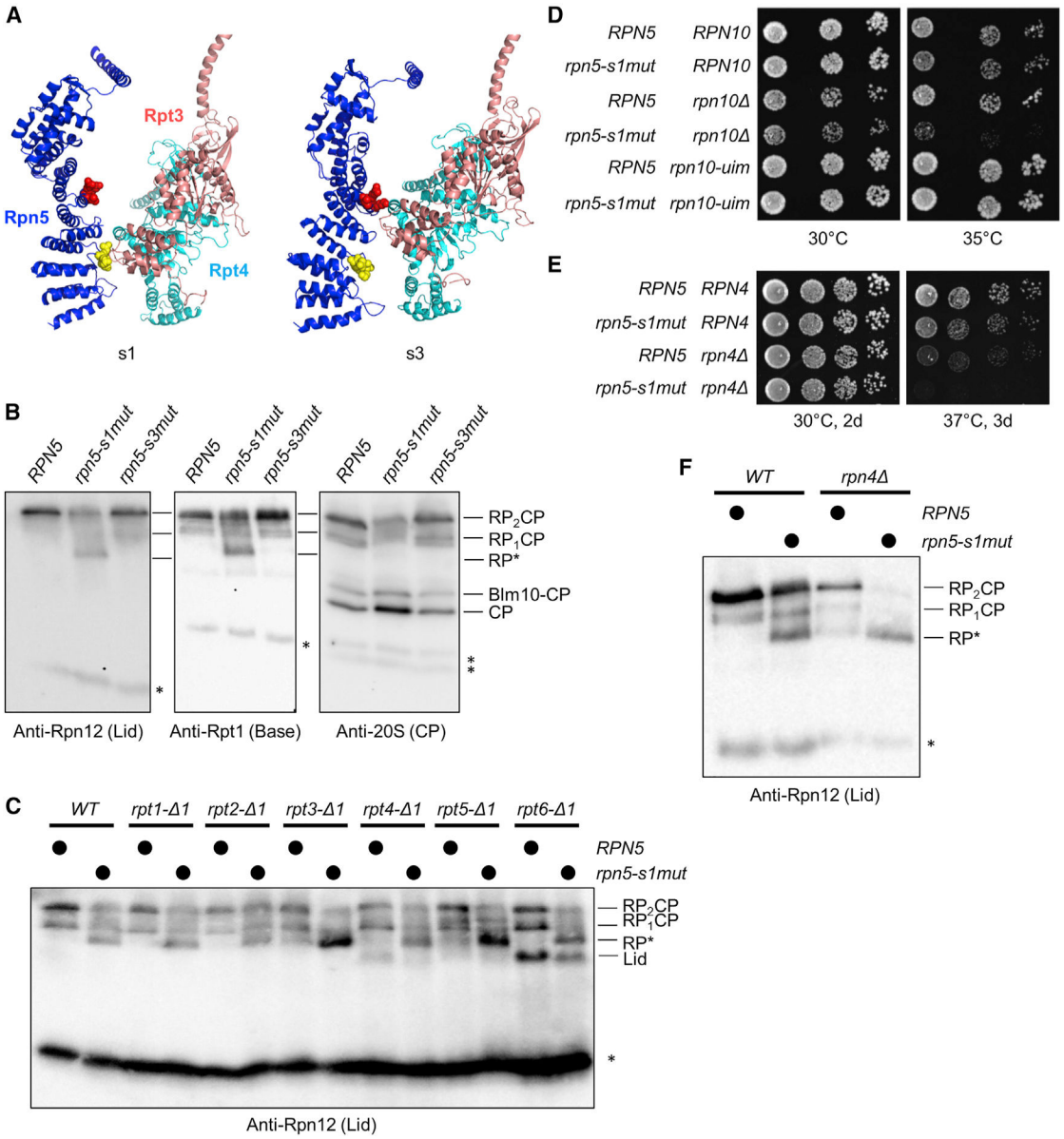

Figure 2. Analysis of Rpn5-Base Contact Point Mutants Reveals a Role for Rpn5 in RP-CP Stability

(A)Engineering conformation-specific mutations to the Rpn5-base interface. Rpn5 residues E127, N128, and K129 (yellow spheres) contact the base in the s1 state, but not the s3 state. Rpn5 residues V198, R201, and K205 (red spheres) contact the base in the s3 state, but not the s1 state. Subunit coloring is as in Figure 1. Many subunits are omitted for clarity..

(B) Disrupting the s1 Rpn5-base contact causes accumulation of the CP and a RP-like species (RP*). Extracts from the indicated yeast strains were separated by native PAGE and immunoblotted with antibodies against Rpn12, Rpt1, or the CP (n > 4). Asterisk indicates assembly intermediate..

(C) *rpn5-s1mut* is synthetic sick with mutations that weaken RP-CP association. Extracts from the indicated strains were separated by native PAGE and immunoblotted with antibodies against Rpn12 (n = 2). Asterisk indicates free Rpn12..

Author Manuscript Author Manuscript Author Manuscript Author Manuscript

(D and E) Equal numbers of *RPN5* or *rpn5-s1mut* cells harboring the indicated *RPN10* (D) or *RPN4* (E) alleleswere spotted in 6-fold serial dilutions on YPD plates and incubated for 3 days or as indicated (n = 3)..

(F) Extracts from the indicated strains were separated by native PAGE and immunoblotted with Rpn12 antibody (n = 3). Asterisk indicates free Rpn12..

See also Figure S2.

Author Manuscript Author Manuscript Author Manuscript Author Manuscript

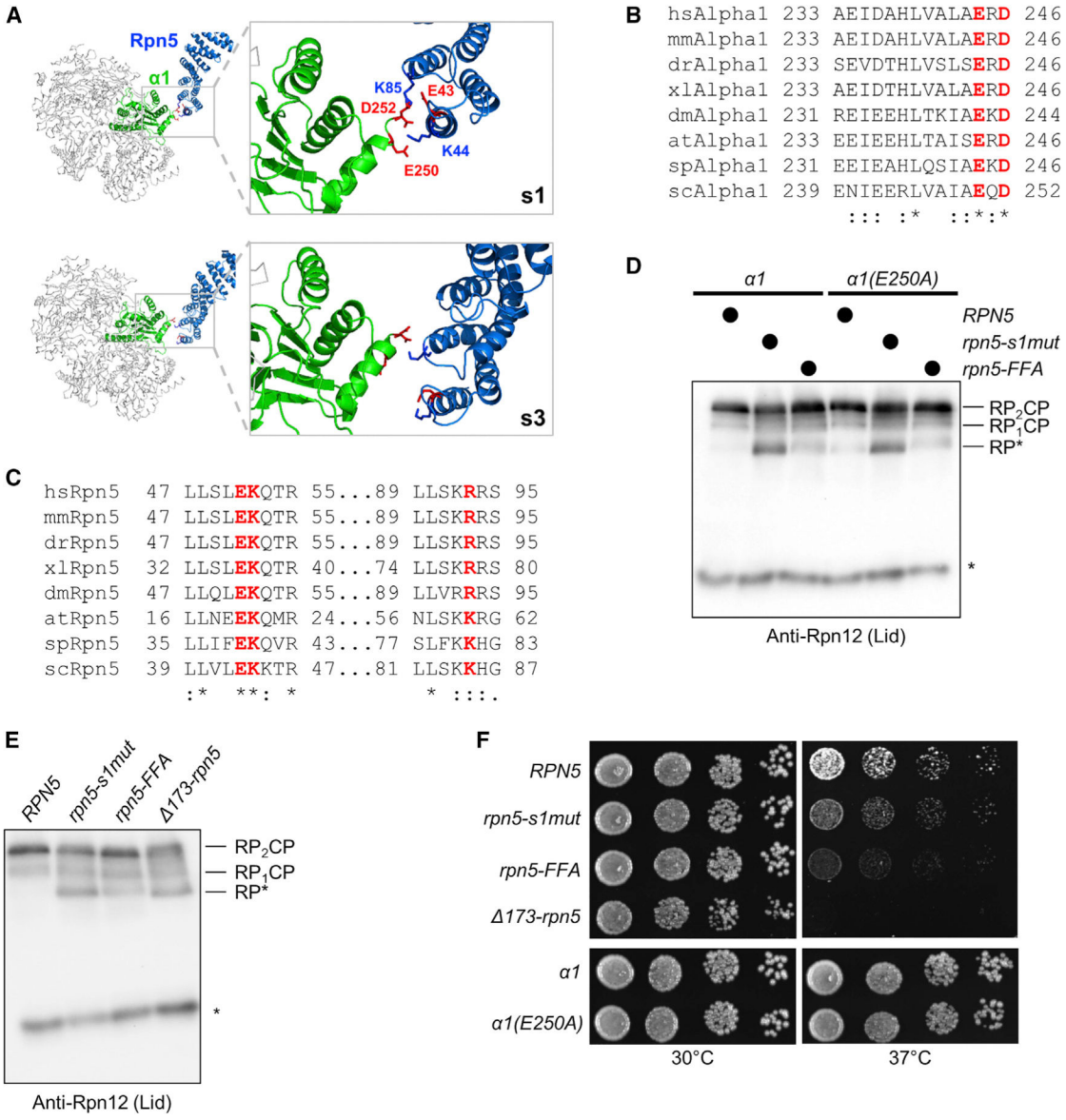

Figure 3. Disrupting Rpn5 Contact with the CP Fails to Phenocopy the *rpn5-s1* Mutation

(A) Potential network of salt bridges between the lid subunit Rpn5 (blue) and the α1 subunit of the CP (green) are evident in thes1 state (PDB: 4CR2), but notthes3 state (PDB: 4CR4). Insets highlight the amino acids contributing to the salt bridges in the s1 state and their positions in the s3 state..

(B and C) Multiple species alignment of α1 (B) and Rpn5 (C) regions contributing the salt bridges shown in (A). Putative salt bridge residues are in red font..

(D) Extracts from the indicated strains were separated by native PAGE and immunoblotted with Rpn12 antibody (n > 3)

(E) Comparison of RP* accumulation in *RPN5* mutants. Extracts from the indicated strains were separated by native PAGE and immunoblotted with antibodies against Rpn12 (n > 3)

(F) Equal numbers of cells from the indicated yeast strains were spotted in 6-fold serial dilutions on YPD plates and incubated as shown for 2 days (n = 3). See also Figure S3.

Author Manuscript Author Manuscript Author Manuscript Author Manuscript

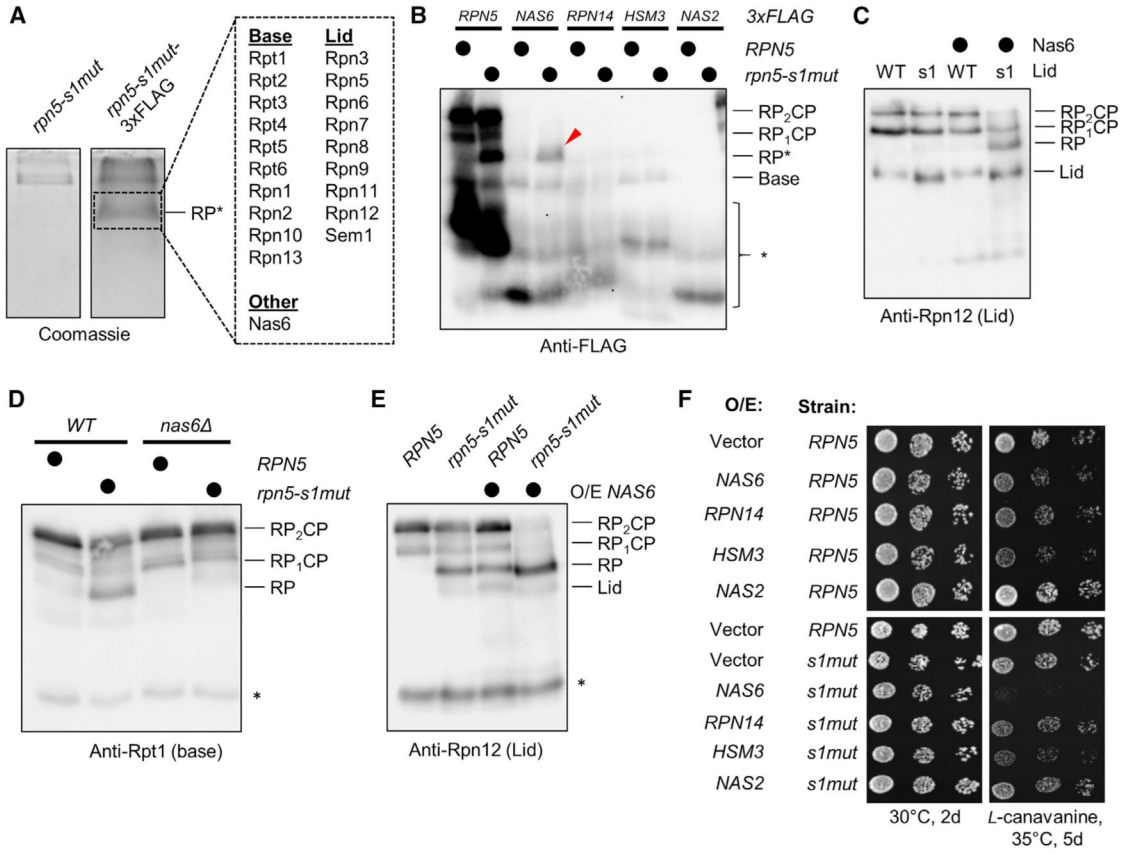

Figure 4. Nas6 Is Required for the *rpn5-s1mut* RP-CP Defect

(A) RP-like species (RP*) was purified from *rpn5-s1mut* cells and separated by native PAGE. The gel was stained with Coomassie, and RP* (boxed) was excised and analyzed by LC-MS/MS. Identified proteins are listed in the box. Nonadjacent lanes from the same gel are shown.

(B) 3×FLAG-tagged proteins were immunoprecipitated from extracts of the indicated yeast strains and separated by native PAGE and anti-FLAG immunoblotting (n = 2). A red arrowhead indicates the position of RP* copurifying with Nas6. Asterisk indicates assembly intermediates.

(C) Nas6 interfereswith 26S proteasome assembly only when the Rpn5 s1 contact is disrupted. Purified CP, *nas6Δ* yBase, Rpn10, and lid harboring either WT or s1mut Rpn5 (s1) and Nas6 as indicated, incubated for 15 min at 30°C, and analyzed by native PAGE and anti-Rpn12 immunoblotting (n > 4).

(D) *NAS6* deletion suppresses the *rpn5-s1mut* defect. Extracts of the indicated strains were separated by native PAGE and immunoblotted for Rpt1 (n = 3). Asterisk indicates assembly intermediate.

(E) Extracts of the indicated yeast strains transformed with empty vector or a high-copy plasmid encoding *NAS6* were separated by native PAGE and immunoblotted with antibodies against Rpn12 (n = 2). Asterisk indicates free Rpn12.

(F) Equal numbers of *RPN5* or *rpn5-s1mut* cells expressing the indicated proteins from high-copy plasmids were spotted in 6-fold serial dilutions on the indicated media (n = 3). See also Figure S4 and Tables S4–S6.

Author Manuscript Author Manuscript Author Manuscript Author Manuscript

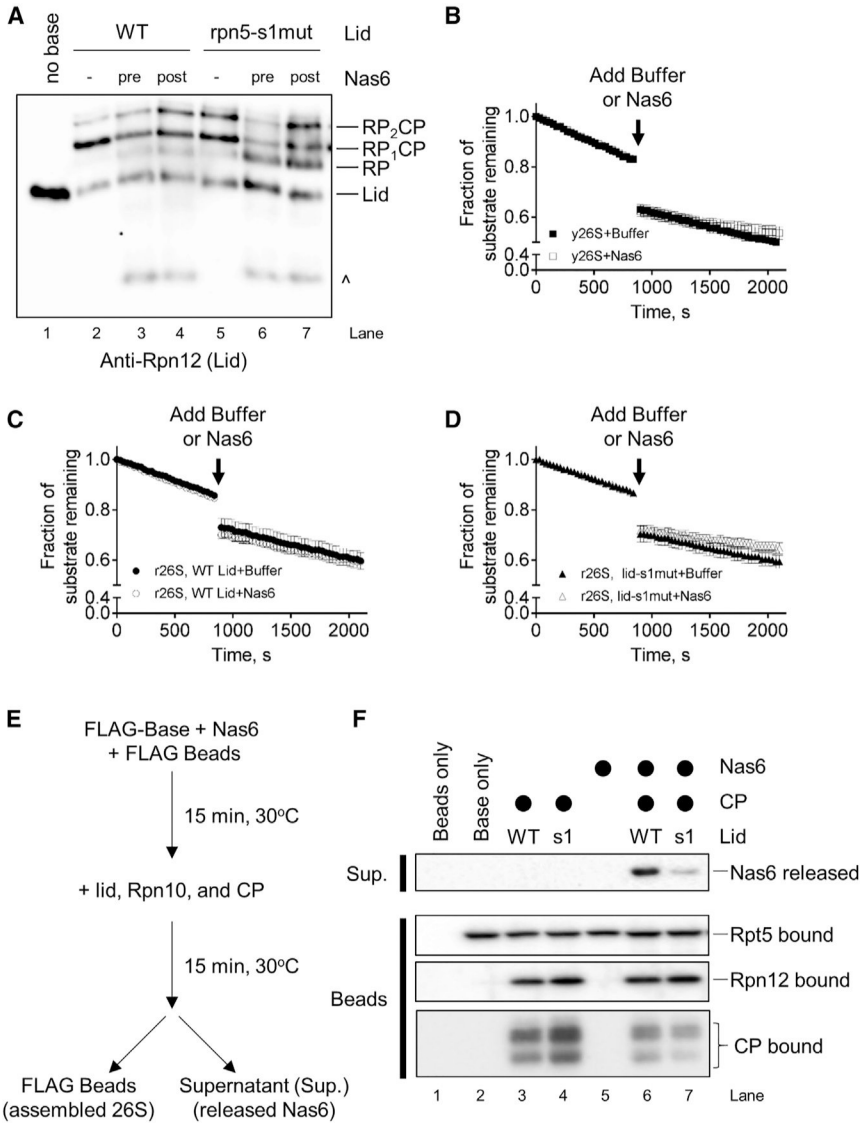

Figure 5. Mutation of the Rpn5 s1 Contact Compromises Eviction of Nas6 from Nascent 26S Proteasomes

(A) Nas6 must be present before *rpn5-s1mut* proteasome assembly to impair RP-CP interaction. Nas6 was added to base before (pre) or after (post) addition of CP, Rpn10, and either WT or s1mut lid. Samples were separated by native PAGE and immunoblotted with an antibody against Rpn12 (n > 4). ^, weak cross-reactivity of the Rpn12 antibody to recombinant Nas6.

(B–D) Addition of Nas6 does not alterthe activity of mature proteasomes. Destruction ofUb_4-GFP-Tail by mature 26S proteasomes purified from yeast (y26S; B); partially recombinant 26S proteasomes (r26S) reconstituted from CP, base, Rpn10, and WT lid (WT lid) (C); or r26S with *rpn5-s1mut* lid (lid-s1mut) (D) was measured under multiple turnover conditions. At the point indicated by the arrow, either buffer control or purified Nas6 was added, and the reaction was continued. No significant difference in the reaction rates were observed between buffer control and Nas6, indicating that proteasomes remained intact after Nas6 addition (n = 3).

Author Manuscript Author Manuscript Author Manuscript Author Manuscript

(E) Schematic of Nas6 eviction assay.

(F) Disruption of the Rpn5 s1 contact compromises Nas6 eviction. Immobilized base-Nas6 complexes were incubated with the indicated proteins before separation into supernatant and bead fractions by centrifugation. Proteins in the supernatant or bead fractions were then separated by SDS-PAGE before immunoblotting for the indicated proteins (n = 2). Blots of the supernatant or beads are indicated to the left.

See also Figure S5.

Author Manuscript Author Manuscript Author Manuscript Author Manuscript

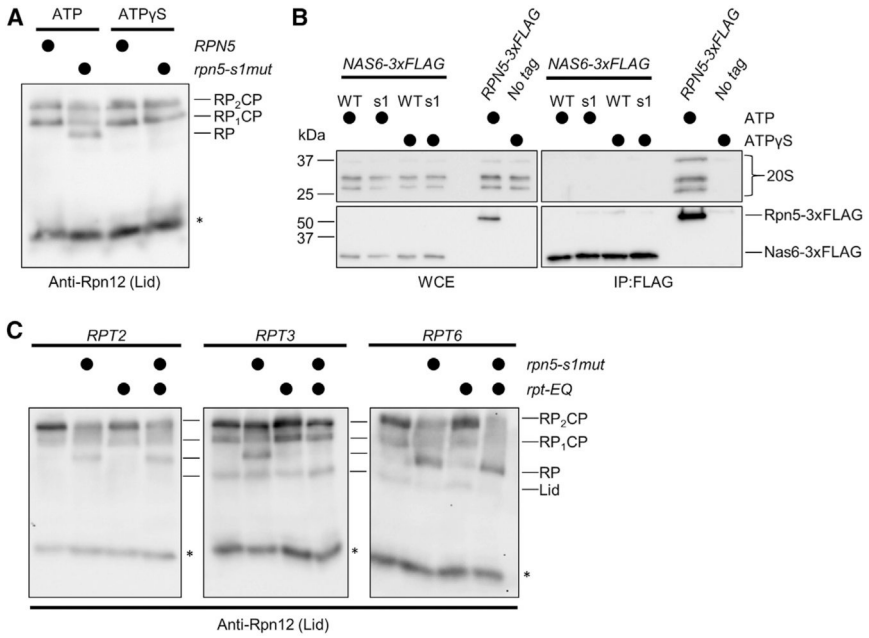

Figure 6. Nucleotide Binding State of Rpt3 and Rpt6 Controls Rpn5-Dependent RP-CP Stability

(A) ATP hydrolysis is required for the RP-CP stability defect. Extracts from the yeast strains indicated were separated by native PAGE in the presence of ATP or ATPγS and immunoblotted with antibody against Rpn12 (n = 3). Asterisk indicates free Rpn12.

(B) Nas6–3×FLAG does not coprecipitate CP subunits. Nas6–3×FLAG and associated proteins were immunoprecipitated from extracts of WT or *rpn5-s1mut* yeast in the presence of ATP or ATPγS. Immunoprecipitates from *RPN5*-3×FLAG and untagged cells served as positive and negative controls for CP copurification, respectively (n = 3).

(C) ATP binding by proteasomal ATPases differentially affects the *rpn5-s1mut* defect. Extracts from the indicated yeast strains were separated by native PAGE and immunoblotted with anti-Rpn12 antibodies (n > 3). Asterisk indicates free Rpn12..

See also Figure S6.

Author Manuscript Author Manuscript Author Manuscript Author Manuscript

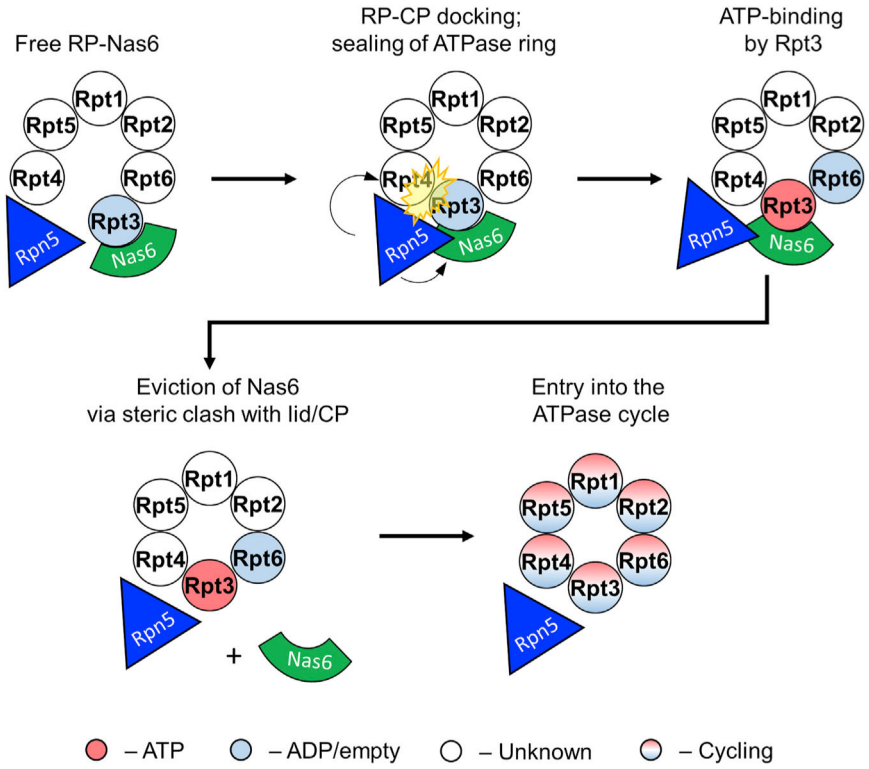

Figure 7. Proposed Model for Rpn5- and Rpt3-Dependent Nas6 Chaperone Eviction

Model for Rpn5- and Rpt3-dependent Nas6 eviction. An opening between Rpt3 and Rpt4 seen in the RP-gankyrin structure accommodates both Rpn5 (blue triangle) and Nas6 (green) and allows docking of the RP-Nas6 complex onto the CP surface. Docking of the RP onto the CP closes the Rpt3 nucleotide binding pocket, allowing ATP binding and an s1-like state to form. The resultant conformational remodeling of Rpt3 leads to Nas6 eviction via steric conflict with the lid and/or CP.

Author Manuscript Author Manuscript Author Manuscript Author Manuscript

Cell Rep. Author manuscript; available in PMC 2019 January 23.

KEY RESOURCES TABLE

REAGENT or RESOURCE	SOURCE	IDENTIFIER
Antibodies		
Anti-Rpt1	Geng and Tansey, 2012	Clone 19S-2
Anti-Rpt5	Enzo Life Sciences	Cat# PW8245; RRID:AB_10555018
Anti-Rpn12	Eisele et al., 2018	N/A
Anti-20S	Enzo Life Sciences	Cat# PW9355; RRID:AB_11177757
Anti-GFP	Roche	Cat# 11814460001; RRID:AB_390913
Anti-FLAG	Sigma Aldrich	Cat# F3165; RRID:AB_259529
Anti-β-actin	Sigma Aldrich	Cat# A5441–1VL; RRID:AB_476744
Anti-Nas6	Funakoshi et al., 2009	N/A
Anti-Rpn14	Funakoshi et al., 2009	N/A
Anti-Nas2	Funakoshi et al., 2009	N/A
Anti-Hsm3	Funakoshi et al., 2009	N/A
Anti-ubiquitin	Santa Cruz Biotech	Cat# sc-8017; RRID:AB_628423
Anti-V5	Life Technologies	Cat# 46–0705; RRID:AB_2556564
Anti-glucose-6-phosphate dehydrogenase (G6PD)	Sigma Aldrich	Cat# A9521–1VL; RRID:AB_258454
Bacterial and Virus Strains		
TOP10F’	Life Technologies	Cat #C303003
LOBSTR-BL21 (DE3)	Kerafast	Cat # EC1001
Chemicals, Peptides, and Recombinant Proteins		
Adenosine triphosphate (ATP)	Sigma-Aldrich	Cat# A2383
Adenosine 5′-[γ-thio]triphosphate (ATPγS)	Enzo Life Sciences	Cat# ALX-480-066-M005
3× FLAG® Peptide	Sigma-Aldrich	Cat# F4799
ANTI-FLAG® M2 Affinity Agarose Gel	Sigma-Aldrich	Cat# A2220
Creatine phosphokinase	Sigma-Aldrich	Cat# CK-RO Roche
Creatine phosphate, disodium salt	Sigma-Aldrich	Cat# 2380 EMD MILLIPORE
Suc-LLVY-AMC	R&D Systems	Cat# S28005M
Gelcode Blue stain reagent	Thermo Scientific	Cat# 24592
5-fluoroorotic acid	RPI Corp.	Cat# F10501–10.0
Experimental Models: Organisms/Strains		

Author Manuscript
Author Manuscript
Author Manuscript
Author Manuscript

REAGENT or RESOURCE	SOURCE	IDENTIFIER
S. cerevisiae strain RTY1 (aka MHY500)	Chen et al, 1993	N/A
For isogenic mutants of RTY1 used herein, see Table S1.	This study	N/A
Recombinant DNA		
For plasmids used herein, see Table S2.	This study	N/A
Software and Algorithms		
Prism 7	GraphPad	https://www.graphpad.com/scientific-software/prism/
Image Lab	Bio-Rad	http://www.bio-rad.com/en-us/product/image-lab-software?ID=KRE6P5E8Z
Pymol	Schrödinger	https://pymol.org/2/
UCSF Chimera	Pettersen et al., 2004	http://www.cgl.ucsf.edu/chimera/

Cell Rep. Author manuscript; available in PMC 2019 January 23.